2019

Designing a modified Zeeman slower for the Paschen-Back magnetic regime

Leo Michael Nofs

Designing a Modified Zeeman Slower for the Paschen-Back Magnetic Regime

by

Leo Michael Nofs

Thesis

Submitted to the Department of Physics and Astronomy

Eastern Michigan University

in partial fulfillment of the requirements

for the degree of

MASTER OF SCIENCE

in

Physics

Thesis Committee:

Éric Paradis, PhD, Chair

Ernest Behringer, PhD

Jonathan Skuza, PhD

Georg Raithel, PhD, University of Michigan

July 15, 2019

Ypsilanti, Michigan

Dedication

I dedicate this document to the friends and family who helped me through this project. Without the love, support, and patience of Charles and Rosalie, I would not have made it this far. Thank you.

Acknowledgments

I am deeply thankful that my friends and family were able to help support me during this research. I was able to count on them during the hardest crunch times, and I have them to thank for my success in this journey.

I would like to thank Dr. Éric Paradis, for giving me the wonderful opportunity to obtain valuable research lab experience with the Raithel group at the University of Michigan. He introduced me to the fascinating field of Atomic, Molecular, and Optical (AMO) Physics, which I found a great passion for. His patience with me during this research is something I am deeply thankful for. I would also like to thank Dr. Georg Raithel for allowing me to work in his lab and gain many new experiences. Lastly, I would like to thank Michael Viray and Lu Ma, the senior graduate students who made me feel welcome in the lab and shared their vast knowledge of working in a research lab.

Abstract

Controlled study of high-density plasmas, such as those found in fusion reactions and stars, is difficult due to their highly-magnetized environments. A specialized high magnetic field (High-B) trap was developed at the University of Michigan in Georg Raithel's research group to study such highly magnetized, high density plasmas using rubidium atoms. By replacing the atom source with a Zeeman slower, a well-studied device to slow and cool atoms, the atom flux could be increased by a factor more than 1000, leading to higher High-B plasma densities. The goal of this project is to design a Zeeman slower that differs from standard designs by accounting for the considerable fall-off bias field from the High-B trap. We created a Python model that computes the modified magnetic field generated by a set of solenoids with operating and design parameters which can be optimized to match the desired Zeeman field within 4 G. This Zeeman slower design allows for operation with or without the High-B bias field.

Table of Contents

List of Figures

Chapter 1: Introduction

A specialized strong magnetic field atomic trapping/plasma chamber was developed by Dr. Georg Raithel at the University of Michigan to study and characterize plasmas and atoms confined under strong magnetic field conditions.[1–7] This device, known here as the High-B apparatus, is capable of achieving an atom trap within fields ranging up to 2.9 T.[1] One particular goal of these experiments was to work towards the observation and measurement of Three Body Recombination (TBR) in this strong field regime, which has been predicted theoretically but not yet observed.[8,9] The trap should enable the observation of TBR in the high-magnetic field regime but was unable to do so in part due to low plasma density.[7] The High-B apparatus used a Low Velocity Intensive Source (LVIS)[10] to inject atoms into the high-field region, which provided an atomic flux of 5×10^8 per second.[5] Increasing the plasma density within the High-B chamber would allow further experiments to observe TBR, as well as study dipole blockade interactions in a strong field[11] (including spatial imaging of the blockade using magnetic lensing), Rydberg quadrupole interactions,[12] and plasmas in the strong-coupling regime.[13]

I have designed a modified σ^+ (decreasing field) Zeeman slower that will provide an increased atom flux to generate denser plasmas within the existing High-B experimental chamber. Zeeman slowers have been proven to be capable of producing a flux greater than 10^{12} atoms per second when working with standard Magneto-Optical Traps (MOTs).[14,15] Standard MOTs have either zero magnetic field at the trap location or a weak bias field (typically under 0.02 T).[16] This increased flux will increase the plasma density and allow

for characterization of the non-linear behavior previously observed in the trap.[1,4] There are currently no known atomic slowing devices that have been designed for use in such strong magnetic fields as created by the High-B chamber.

Phillips and Metcalf first showed in 1982 that a counter-propagating laser beam of fixed frequency shining on an incident stream of atoms will slow the hot atoms down from thermal velocities (typically over 1500 mph (670 m/s)) to under 45 mph (20 m/s).[17] Typical atomic sources used for trapping experiments involve heating a metallic source until it vaporizes into a gas within the vacuum system. The velocity distribution is characterized by a Boltzmann curve and depends on how the hot gas leaves the oven.[18] As the atoms slow down, the Doppler effect causes them to interact with the slowing laser at a lower frequency. This change in frequency is known as a Doppler shift. There is a limit to how large a shift can take place before the atoms are no longer able to interact with the slowing laser.[16] This limit arises from the Gaussian distribution of intensity over frequency and laser cavity modes.[19]

If the atomic transition energy between the ground and excited states of the atom is equal to the energy of the incident light, they are said to be on resonance. Therefore, the Doppler shift will cause the frequency in the atom's frame of reference to be larger, shifting it out of the resonance condition. This effect depends upon the velocity, so it will change as the atoms decelerate. The atomic transition energy is also impacted by the presence of an external magnetic field through the Zeeman shift. The Zeeman shift is caused by the interaction of an external magnetic field with the spin magnetic dipoles of the protons,

neutrons, and electrons. Magnetic dipoles have a tendency to align either parallel or anti-parallel to an external magnetic field, which changes the energy of the system.[20–22] The internal interaction between orbital and nuclear spin creates the hyperfine structure. When an external magnetic field is applied, these hyperfine energy levels will change based on the dot product of the magnetic field and the angular momentum operators of the atom to create the Zeeman energy levels. The change in energy for any particular hyperfine level due to an external magnetic field is known as a Zeeman shift. The Zeeman shift from a spatially varying magnetic field can then compensate for the Doppler shift and keep the atoms on resonance. Such a device that balances the Doppler and Zeeman shifts is known as a *Zeeman slower*, and the design and modeling of a modified slower is the focus of my research.[16]

The Zeeman slowing technique has been well optimized in recent years.[23–27] The effects of the apparatus design on field profile have been thoroughly studied, with the primary design philosophy requiring a constant deceleration throughout the slower. There is a limit to the atomic deceleration which corresponds to a limit to the gradient of the magnetic field. This limitation is called the adiabatic requirement which arises from the maximum rate of energy change allowed to maintain resonance between the laser and atomic transition frequency.[28] Failing this requirement will result in a Zeeman shift out of resonance with the laser, and the loss of atoms into dark states (ones that no longer can be excited by the slowing laser).[16] Since this adiabatic requirement depends on the gradient of the magnetic field, the shape of the field isn't unique. Because the force the laser exerts on

the atoms is velocity dependent, it is difficult to analytically calculate the acceleration. The solution is typically obtained by using a frame of reference that is constantly decelerating and based on atoms with the correct velocity to be resonance in the presence of the external magnetic field from the Zeeman coils.[16,25,28–30] There are three standard types of Zeeman slowers based on the polarization of the slowing laser and the sign of the magnetic field gradient (whether the field increases or decreases in magnitude).

The light is circularly polarized and denoted by $\sigma^{+/-}$ (see Figure 2.2 for orientations) and drives a transition that links two states with an energy difference equal to that of one photon from the slowing laser based on the frequency/wavelength.[28–30] The total angular momentum of the state will change by one unit. The hyperfine state of the ground level with the highest transition energy is driven by σ^+ light, while the lowest energy transition is driven by σ^-. When the laser beam direction is parallel with the magnetic field axis and is circularly polarized as σ^+, this corresponds to the first type of Zeeman slower. The field profile will be decreasing in order to obtain the desired slowing effect. When the laser beam is σ^- polarized and anti-parallel to the magnetic field, this corresponds to the second type of Zeeman slower. The third type is termed zero-cross (or spin-flip), which combines the two. As its name implies, the zero-cross type has a magnetic field that crosses zero along the length of the slower, which requires additional optics and re-pumping to prevent the atoms from dropping out of the slowing resonance.[14,26] The laser direction needs to be opposite to the atomic motion; otherwise, the atoms will accelerate away from the atomic source (rather than slowing down). The slowing of rubidium with σ^-

light has been previously investigated and detailed in publications by Dedman, Barrett, Mayer et al., Slowe, among many others.[14,25,29,31] I will discuss each type of Zeeman slower in additional detail in the Methods chapter.

The proposed slower will utilize a decreasing field (σ^+) profile as there are additional complications that prevent using an increasing field profile and the spin-flip design would pose issues with atoms falling out of trappable states. While an increasing field profile would better fit the shape of the High-B fall-off field, such a slower uses atomic sub-states which are not able to be trapped.[32] The designed slower is unique because it loads a continuous stream of atoms into the High-B trap, which is a unique atom/plasma trap. A solenoid was designed to generate a magnetic field that, when summed with fall-off field from the High-B trap, produces a net field equal to that of a standard Zeeman slower. Additionally, the gradient of this net field must be smooth enough to ensure the adiabatic following condition (adiabaticity) is met to maximize the number of atoms into the High-B chamber the trapping of and subsequent plasma generation. To ensure the atoms reach the trap, they will exit the slower with the required kinetic energy to reach the trap, taking into account the energy lost to the magnetic field.[1]

The goal is to design a modified Zeeman slower which is able to operate under four separate conditions: rubidium atoms with the High-B active (producing the large bias field), rubidium atoms without the High-B active (no bias field), strontium atoms with the High-B active, and strontium without the High-B. The cases without the High-B active are just the standard ideal Zeeman slower designs for rubidium and strontium.[15,31,33] All four

of these conditions will utilize the same coil pack geometry but will have different currents running through the coil packs. The primary focus is to design a slower for rubidium while investigating the feasibility of slowing strontium as well. As will be discussed in Section 3 later, it is impractical to design a single device for the slowing of both rubidium and strontium.

To obtain the desired field profile, the standard tapered solenoid approach will be used with controllable and modular coil packs. Having a modular design will allow for variations in the trapping field strength as well as the use of different atoms/isotopes. Steps to optimize the slower based on previous work will be taken.[24,25,27] This slower will be unique as it will use the large fringe field from the High-B chamber as the majority of its slowing field. The main trapping field reaches a strength of 2.6 T under standard operating conditions, so the magnetic field magnitude will continue to increase after the atoms exit the slower, unlike standard MOTs which approach very low magnitude fields for trapping. The challenges of this project will be matching the coil field to this fringe field so that there are not significant losses due to atoms falling out of resonance.

There is currently an operational Zeeman slower in the Raithel research laboratory at the University of Michigan which was built by Mhaskar, but it was designed specifically to work for the ^{87}Rb isotope and uses the zero-crossing configuration.[26] With the High-B field being as strong as it is, there is a roughly 160 G field at the planned exit point for the slower. In comparison, Mhaksars slower would have a field strength of -82 G at the same point. It would be too difficult to modify the existing slower to compensate for the

presence of the High-B fall-off field as it was not designed with that in mind. This other slower also was designed to load a standard MOT, which requires a lower output velocity and magnetic field strength.[26]

The design of this modified Zeeman slower must also prove physically viable for real world constraints and considerations. These design constraints will be discussed later on. The values for the High-B bias field are obtained from existing FORTRAN code previously used to model the High-B chamber's magnetic field. Designing the modified slower involved creating a complete computational model in Python that calculated the magnetic field from a pack of coiled wires using the Biot-Savart law. This coil pack model was then optimized based on physical parameters and constraints in order to fit the magnetic field profiles of the ideal Zeeman magnetic field and that of the coil packs (with or without the bias, depending on the desired mode of operation).

Chapter 2 describes the methods used and is comprised of four subsections: the first subsection is a description of the mechanisms that define and limit the Zeeman slowing process; the second is a description of how those mechanisms are typically used with the three main standard types of Zeeman slowers; the third is a description of the main modification of the Zeeman slower; and the fourth is a description of how everything was modeled in Python including details of my optimization process. Finally, there is also a brief discussion how the heat generation was modeled to ensure the system would not overheat given the design specifications.

Chapter 3 describes the results and is comprised of two subsections describing the

resulting optimized design and details of how my Python algorithm obtained them. There were significant computational challenges with optimizing so many parameters, which I discuss in this section.

Chapter 4 is a summary of research and design work I have completed and includes a discussion the state of the design with regards to the steps required for construction.

There are Appendices for the derivation of the full Biot-Savart model that I used for the magnetic field calculations as well as an in-depth discussion of the hyperfine structure and how it applies to the cycling transition, particularly of rubidium. I also discuss how to do the hyperfine calculations using Python as I personally had significant difficulty ensuring the excited energy levels were properly calculated.

So let us begin with the two most important questions to answer first: What is a Zeeman slower and how does it work?

Chapter 2: Methods

The application of standard Zeeman slowers have been well discussed and optimized.[17,25,28,29,31] I have designed a modified Zeeman slower which will be used with the High-B chamber. In this chapter, I will first discuss the atomic structure of the atom and how it behaves within an external magnetic field. In these conditions, rubidium can be treated as a two-level system. I will then discuss what this means for the design goal of reducing the mean velocity of the incident atoms. Then I derive the ideal Zeeman field along with the constraints involved. Then I will discuss how this modified Zeeman slower will utilize the fall-off bias from the High-B chamber. Lastly, I will cover the numerical model I created in Python to simulate the magnetic field generated from a solenoid and how I optimized the combination of many solenoids to fit the magnetic field profiles that would slow the atoms as expected.

2.1 The Ideal Zeeman Slower

The technique of Zeeman slowing is based upon the principle of radiative force, which is the force an atom experiences due to the spontaneous absorption, followed by emission, of a photon. For a two level system (or an effective two-level system, as selection rules limit our cycling transition to be), this force is defined as:[16]

$$F = \frac{\hbar k \Gamma}{2} \frac{s_o}{1 + s_o + 4(\delta/\Gamma)^2} \tag{2.1}$$

where $s_o = I/I_S$ is the saturation parameter and is the ratio of the laser intensity to the transition saturation intensity, k is the wave-number of the laser, $\Gamma = 1/\tau$ is the linewidth (inverse of the excitation lifetime, τ), and δ is the total detuning difference between the atoms and the laser light. This force comes from the transfer of momentum between the photon and atom and is related to the scattering rate. The scattering rate, γ_P, is a Lorentzian with respect to the detuning, δ, and given as

$$\gamma_P = \frac{s_o \Gamma/2}{1 + s_o + \frac{4\delta^2}{\Gamma^2}} \tag{2.2}$$

which, for circularly polarized light, gives us a force equation neatly defined by $\vec{\mathbf{F}} = h\vec{\mathbf{k}}\gamma_P$. The scattering rate is a function of both laser detuning and intensity. This detuning is given by[16,25,26]

$$\delta = \omega_l - \omega_a - \delta_D \tag{2.3}$$

with ω_l being the frequency of the laser, ω_a the frequency of the atomic transition, and δ_D being the Doppler shift in light frequency experienced by the atoms. The Doppler shift is the change in laser frequency that the atoms experience from the moving reference frame of the atom with velocity $\vec{\mathbf{v}}_a$ and is given by $\omega_{l'} = \omega_l - \vec{\mathbf{k}}_l \cdot \vec{\mathbf{v}}_a$. It is typical to write Doppler detuning as[16]

$$\delta_D = -\vec{\mathbf{k}}_l \cdot \vec{\mathbf{v}}_a \tag{2.4}$$

so as to define it as a velocity-dependent difference in the frequency. We will treat the atomic frequency ω_a in a similar manner by breaking it up into the zero-field, zero velocity transition frequency, ω_o and the shift caused by an external field, $\Delta\omega_{field}$. For a magnetic field, $\Delta\omega_{field}$ is known as the Zeeman Shift and is given by[21,22]

$$\Delta\omega_{Zeeman} = \pm\frac{\boldsymbol{\mu'}}{\hbar} \cdot \vec{\mathbf{B}} \tag{2.5}$$

where $\boldsymbol{\mu'}$ is the magnetic moment of the transition. The value of $\boldsymbol{\mu'}$ depends on the Lande g-factors for the ground and excited states of the atom and is defined as $g_F m_F \mu_B$ when in low magnetic fields (known as the Zeeman regime). Stronger magnetic fields fields (known as the Paschen-Back regime) causes a decoupling effect between the $|Jm_J Im_I\rangle$ states and is more complicated to solve. Solving for the intermediate field is computationally difficult as it requires re-diagonalizing the hyperfine and interaction (from the laser) Hamiltonians for every magnetic field value. I used this last method to solve for the energy levels in my system.[16]

For ^{85}Rb, which utilizes the cycling transition of $|F = 3, m_F = \pm 3\rangle \Rightarrow |F' = 4, m_{F'} = \pm 4\rangle$, we have $g_{F=3} = 1/3$ and $g_{F'=4} = 1/2$ for the ground and excited states, respectively.[16] F is the total angular momentum of a system defined as the sum of the spin, orbital, and nuclear angular momenta, denoted by $\vec{\mathbf{S}}, \vec{\mathbf{L}}$, and $\vec{\mathbf{I}}$, respectively. The cycling transition refers to states that are linked together in the presence of the slowing laser (based on polarization). For ^{85}Rb, a laser of 780.24 nm has enough energy to link the $\left|5S_{1/2}\right\rangle$ ground state, $|g\rangle$, with the $\left|5P_{3/2}\right\rangle$ excited state, $|e\rangle$.

Circularly polarized light will change the electron angular momentum by ±1, provided there is a transition available to a higher/lower state.[21,22] We can take advantage of this after lifting the degeneracy by applying a magnetic field before shifting the laser frequency so that it interacts with only one of the Zeeman sub-levels. To cycle (i.e., to optically pump) a transition, it is typical to utilize circularly polarized light and ground level states which only have one excited state that can be populated.

These Lande-factors work out such that $\boldsymbol{\mu'} = \pm\mu_B$ for the states of the cycling transitions. The positive sign corresponds to the m_F states with a positive value, and the negative corresponds to those with a negative value. The ratio $\frac{\mu_B}{\hbar}$ is approximately 14.4 GHz/T and defines how the resonant frequency for the transition shifts with magnetic field. In general, this results in the Zeeman shift of the frequency of

$$\Delta\omega_{Zeeman} = \pm\frac{\mu_B}{\hbar}\left|\vec{\mathbf{B}}\right| \tag{2.6}$$

where sign of the Zeeman shift depends upon which cycling transition is used and is determined by the polarization and orientation of the light with respect to the atomic velocity. To drive these transitions (known as the D2 transition, as seen in Figure 2.1) for both species of rubidium, a laser with a wavelength of 780.24 nm is used.[16] The hyperfine structure is discussed in further detail, including all Clebsch-Gordon coefficients required to calculate the Zeeman shift for the rubidium states $5S_{1/2}$ and $5P_{3/2}$, in Appendix A.

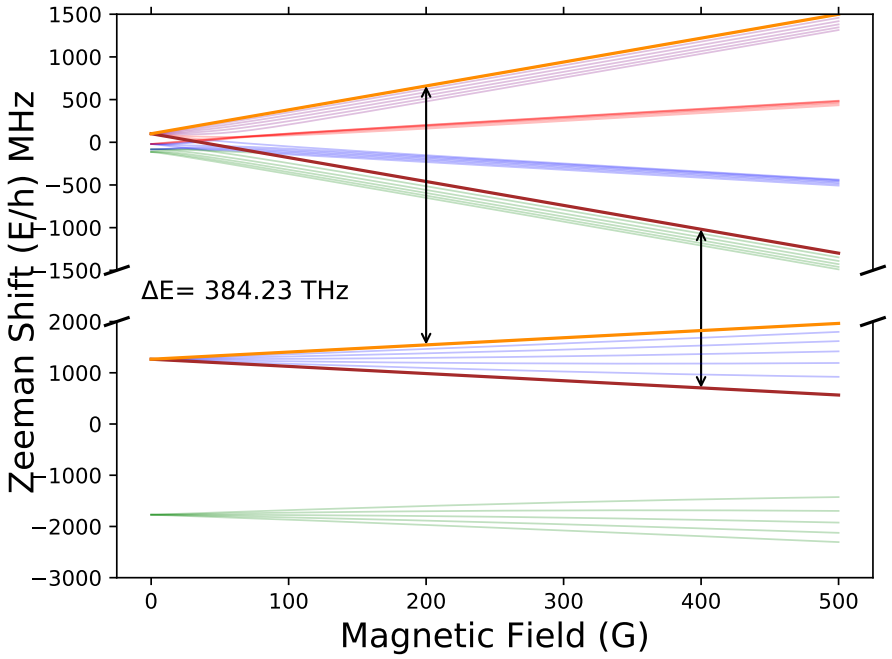

Figure 2.1: Cycling Transitions for Rubidium Zeeman Slower. Selection rules limit transitions to cases where $\Delta m_F = 0,\pm 1$. By using circularly polarized light, we require a change of ± 1 to the angular momentum per interaction. The top half of the plot contains the hyperfine structure of the $5P_{3/2}$ excited state of ^{85}Rb. The bottom half contains the $5S_{1/2}$ ground state of ^{85}Rb

The standard notation is that the lower (upper) sign corresponds to $\sigma^-(\sigma^+)$ slowers, and is with reference to the laser propagation.[29,31] Figure 2.2 shows the the difference between the two forms of circular polarization. The cycling transitions as seen in Figure 2.1 are driven by using this circularly polarized light. A change in $\Delta m_F = +1$ corresponds to σ^+ light and $\Delta m_F = -1$ to σ^- light. The designed slower uses the σ^+ transition for the upper energy levels.

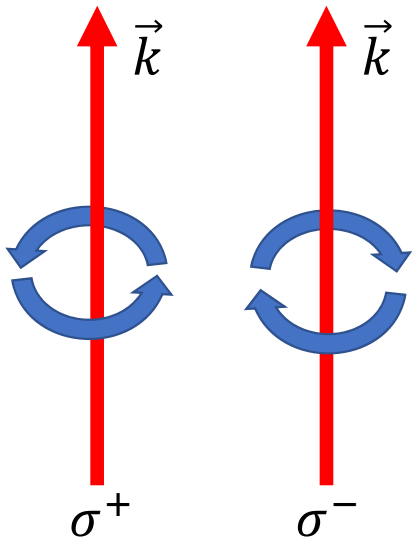

Figure 2.2: Relative orientation of the circular polarization with respect to the slowing laser propagation direction. This is important as the polarization determines the states in the cycling transition, and only low-field seeking states can be trapped.

As will be discussed momentarily, σ^- slower designs have a magnetic field profile that increases in strength as the atoms slow, and σ^+ slowers have a decreasing magnetic field strength. We can then take this relation for the Zeeman shift, along with the Doppler shift, and plug them into the total detuning equation. For the special case of $\delta = 0$, we obtain what is known as the resonance condition[28]

$$\omega_l + \vec{\mathbf{k}} \cdot \vec{\mathbf{v_a}} = \omega_o \pm \frac{\mu_B}{\hbar} \left| \vec{\mathbf{B}} \right| \tag{2.7}$$

where the frequency shift from the atoms slowing down is exactly accounted for by the Zeeman shift, so the incoming light is still able to drive the cycling transition. Being perfectly resonant is not ideal, and it has been shown that the atomic velocity must be

lower than the resonant velocity for the deceleration to maintain stability.[28–31] We observe this by taking our radiative force, Equation 2.1, and solving Newton's second law of motion, $F = ma$, for the atoms. To account for this force being velocity dependent, a reference frame that is uniformly decelerating is used, and we end up with the same detuning equation as in Equation 2.3.[28,30] The mathematics behind this approach are covered in detail by Napolitano.[28]

Solving for the equations of motion for the atom in this decelerating reference frame provides an upper limit to the acceleration, and therefore a limit for the magnetic field gradient as well. This limiting condition is known as the adiabatic following condition.[28,30] The major consequences of this requirement, frequently referred to as the adiabaticity are as follows:

1. The velocity (and acceleration) must be lower than the resonant velocity (and acceleration) for a stable system.

2. The velocity (and acceleration) therefore limits the gradient of the magnetic field.

3. The acceleration will be constant for resonant atoms.

4. Failing to maintain adiabaticity will result in atoms not being slowed.

The maximum acceleration is defined as[16,25,30]

$$a_{max} = \frac{\Gamma \hbar k}{2m} \frac{s_o}{1 + s_o} \tag{2.8}$$

and is what shapes the magnetic field. We use the resonance equation, and with the substitution of $\Delta\omega = \omega_l - \omega_a$, we arrive at an equation relating the positional velocity to the spatial magnetic field profile:

$$v(z) = \frac{1}{k}(\mp\mu' B(z) - \Delta\omega) \tag{2.9}$$

where once again the sign for the magnetic field term depends upon the slower design. These conditions, together with the stability requirement, provide the required shape for the $\sigma^{+/-}$ fields. It is worth noting that the sign convention is tied to the polarization and not the magnetic field strength or gradient.

For this modified slower, we are using the σ^+ configuration and placing the output side of the slower such that the magnetic field required will be almost completely generated by the High-B chamber. If we solve for the magnetic field as a function of the velocity for the σ^+ slower, we get

$$B(z) = \frac{\hbar}{\mu_B}(kv(z) + \Delta\omega) \tag{2.10}$$

which we can then solve by utilizing the constant acceleration assumption in conjunction with the boundary conditions for the velocity. The magnetic field will be tapered and will be of a form that has a maximum of $B_{bias} + B_{taper}$ for $v(z = 0) = v_o$ and a minimum of B_{bias} for $v(z = L) = v_f$, where L is the length of the slower. This field shape is chosen to match the adiabaticity requirements above and has been shown to work in many publications.[24,28,29,31] These velocities are typically experimentally determined by the atom

source characteristics together with the initial velocity and the capture velocities of the trap. We can then use the kinematic equations and velocity extrema to obtain

$$B(v = v_o, z = 0) = B_{bias} + B_{taper} = \frac{\hbar}{\mu_B}(kv_o + \Delta\omega) \tag{2.11}$$

$$B(v = v_f, z = L) = B_{bias} = \frac{\hbar}{\mu_B}(kv_f + \Delta\omega) \tag{2.12}$$

which provide

$$B_{bias} = \frac{\hbar}{\mu_B}(kv_f + \Delta\omega) \quad , \quad B_{taper} = +\frac{\hbar k}{\mu_B}(v_o - v_f) \tag{2.13}$$

and are used to find the ideal Zeeman slower field given by[31]

$$B(z) = B_{bias} \pm B_{taper}\sqrt{1 - z/L} \tag{2.14}$$

which is a wonderfully simple equation to describe the magnetic field. While this equation represents the ideal Zeeman slower field, it is not practical as any imperfection or deviation from the field shown in Figure 2.3 will break adiabaticity and force the atoms out of the slowing process. The standard way to account for these sorts of imperfections and fluctuations is to introduce a design parameter, $\eta < 1$, which limits your acceleration by[25,28,29,31]

$$a_o = \eta a_{max} \tag{2.15}$$

This design parameter helps ensure that our deceleration remains smaller than the maximum, and dictates the length of the slower.

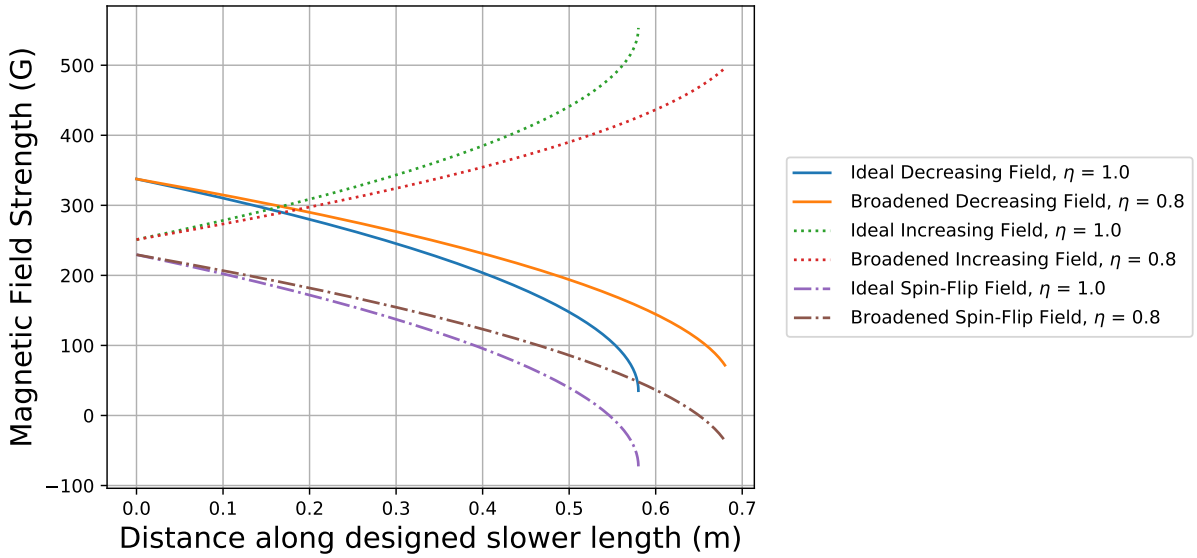

Figure 2.3: Magnetic field profile for σ^- , σ^+, and spin-flip style slowers with η broadening effect. The length of a Zeeman slower is determined by the design parameter, η. The broadened deceleration curve is chosen to allow for variance in the deceleration in a lab setting. Attempting to construct a slower for the $\eta = 1$ case would result in poor performance as any atoms that slowed faster than the maximum deceleration rate would have unstable velocity trajectories and would fall out of the slowing process. This occurs since the Doppler shift would no longer match the Zeeman shift as the atoms have too much velocity. $\eta = 0.792$ is determined by choosing L = 0.68 m and solving Equation 2.16

For an object undergoing constant acceleration with set initial and final velocities, you can decrease the acceleration by having it take place over a longer distance. So as we decrease η, the slower will get longer based on

$$L = \frac{v_o^2 - v_f^2}{2\eta a_{max}} \tag{2.16}$$

where you can set $\eta = 1$ to determine the minimum distance for the slower. Alternatively, you can design a slower with a particular length and extract the corresponding η value instead. The final velocity for the slower needs to match the capture velocity of the High-B

Trap and is typically defined for the on-resonant atoms (experiencing constant deceleration) as

$$v(z) = \sqrt{v_o^2 - 2a_o z} \tag{2.17}$$

and being one of the standard kinematic relations.

For a typical MOT, the output of your Zeeman slower should have the lowest velocity you can with the weakest magnetic field so as to not interfere with the MOT fields.[17] The High-B trap will have a large magnetic potential energy barrier that the rubidium atoms must overcome. This can be thought of as the amount of energy it would take to roll a ball to the top of a hill, which changes based on how far up the hill you start. This magnetic potential energy, U_B, can can be calculated by[34]

$$U_B = -\vec{\mu} \cdot \vec{\mathbf{B}} \tag{2.18}$$

where $\vec{\mu}$ is the magnetic dipole moment and $\vec{\mathbf{B}}$ is the magnetic field being traversed. If we use the assumption that the kinetic energy is zero at the peak of the magnetic field, which coincides with the trap location and design, then we can determine the trapping velocity using energy analysis through the Hamiltonian, $\mathbf{H}$. It is assumed that all other possible energies are small enough to be neglected,

$$\mathbf{H_i} = \mathbf{H_f}$$

$$\begin{aligned} T_i + U_i &= T_f + U_f \\ \frac{1}{2}mv_i^2 + \mu B_i &= \frac{1}{2}mv_f^2 + \mu B_f \\ v_{i,trap} &= \sqrt{2\mu\Delta B/m} \end{aligned} \tag{2.19}$$

where T and U are the kinetic and potential energies, v is the transverse velocity of the particle, and m is the atomic mass. For rubidium atoms with a 2.6 T High-B field, this corresponds to roughly 18.5 m/s. The source for the rubidium atoms is the oven that was designed and built for the previous Zeeman slower in the Raithel research group by Mhaskar.[26] The oven provides an effusive source of roughly 10^{15} hot atoms and is able to produce a velocity profile with a peak velocity of 380 m/s, a standard deviation of 138 m/s, at a temperature of 430 K.[26] We see how decreasing η leads to a longer slower and a broader magnetic field gradient in Figure 2.3. Any designed Zeeman slower must have a gradient less than the $\eta = 1$ case. This gradient can be calculated by taking the partial derivative of the magnetic field given in Equation 2.14 such that

$$\begin{aligned} \frac{\partial B}{\partial z} = \frac{\hbar k}{\mu_B}\frac{\partial v(z)}{\partial z} &= \frac{\hbar k a_o}{\mu_B v(z)} \\ \Rightarrow \left|\frac{\partial B}{\partial z}\right|_{max} &\leq \frac{\hbar k a_o}{\mu_B v(z)} \end{aligned} \tag{2.20}$$

which will remain true so long as $a_o < a_{max}$, and is typically ensured by the use of the design parameter, η.

The last element of the Zeeman slower equation is the total detuning, $\Delta\omega$. Although this is an experimentally determined parameter, there are a few related considerations and limitations. For the σ^- configuration, the total detuning must be negative, and for σ^+ and zero-crossing configurations it must be positive(or zero).[29] Having finished deriving the equations for a standard σ^+ slower, I will now discuss the types of Zeeman slower configurations along with their pros and cons.

2.2 Different Types of Zeeman Slowers

There are three types of Zeeman slowers: σ^+, σ^-, and zero crossing (also denoted spin-flip).[28,29,31] The adiabaticity requirements limit the design of our slower based on two main factors: the orientation of the laser propagation with respect to the atomic velocity direction and whether the magnetic field is increasing or decreasing. This second factor comes from the sign attached to the dipole moment, $\boldsymbol{\mu'}$.

The sign of the Doppler shift, δ_D, is determined by whether the laser is co-propagating the atoms or counter-propagating them. For co-propagation, it means that the wavevector, $\vec{\mathbf{k}}$, and the the atoms are traveling in the same direction, or parallel. Counter-propagation means they are traveling in opposite directions with each other, or anti-parallel. For the counter-propagation configuration, the Doppler shift experienced by the atoms will be positive (negative for co-propagation).[16] For a Zeeman slower, the laser must be counter-propagating with respect to the atoms in order for the force to slow the atoms.

This slower uses a laser counter-propagating the atomic beam. If we look at the hyperfine levels from Figure A.1, we notice several intersections in energy levels. This means we regain degeneracy at that point and could no longer determine which state the atom is in. We want to avoid these interactions as the atoms may hop into the unwanted level as the atom is in a superposition of states at that frequency. This can be done by forcing a greater negative (blue shift) detuning of the σ^+ states with a high bias magnetic field. Revisiting Equation 2.9 and using the negative detuning for the σ^- slowers, we see that the magnetic field must increase in magnitude for the atoms to decelerate.

The σ^+ design is the decreasing field configuration and was the first style used for slowing atoms.[17] This configuration cycles the upper-most states for the transition m_F sublevels. The main drawback is that all of the atoms moving slower than the initial resonant velocity will eventually become resonant with the laser frequency and experience slowing. This is true even for atoms with a negative velocity and makes it exceedingly difficult to ensure the atoms are slowed to the desired velocity.[31] This issue with extraction is made even more difficult for typical MOT systems as the overall magnetic field needs to return near zero for trapping, which mean the hyperfine m_F states become degenerate and could possibly fall into dark states which can not be slowed. The modified slower has no such requirement to lose degeneracy and, as such, can continue to increase the magnetic field into the chamber. This means that any atoms that drop out of the slowing process will not be resonant further down stream as the detuning will become too great for the laser to interact with the atoms.

The zero crossing (or spin flip) design is similar to the σ^+ decreasing field. In practice, a zero crossing slower takes the magnetic field for a decreasing field slower and offsets it such that it will have to cross through a magnetic field zero. This is usually done by having a second, smaller coil setup that has its current traveling opposite in direction to the main solenoid. One of the main advantages of this configuration is that, while the total shift in magnetic field is the same, it takes place at far lower values and therefore requires less current to generate. The primary disadvantage is the inability to distinguish between your states at the zero field point. This means that atoms will drop out of the cycling transition at the zero-cross point. A second laser, deemed the repumper, is added to the setup to excite atoms back into the cycling transition to counteract the losses to dark states. The previous Zeeman slower in the Raithel Lab used this configuration.

The σ^- design, the increasing field configuration, was shown above. Unlike for a decreasing field, the atoms will be resonant throughout the entire slower until they reach the maximum magnetic field. This means that the difficulty in atom extraction caused by atoms being pushed back into the slower does not exist. This configuration is also less prone to fluctuation in the laser frequency and intensity.[31] The typical drawback is caused by the large (relative) magnetic field from the slower output. If you are attempting to load a standard MOT, this field would likely interfere with the trapping field. Decreasing the magnetic field also causes the Zeeman shifted energy levels to mix in the same way they do for the zero-crossing configuration. As the magnetic field from the High-B chamber continues to increase sharply after the slower coils end, this state mixing will not be an

issue for this modified Zeeman slower.

With all of the pieces in place for a standard ideal Zeeman slower field, we can now turn our attention towards implementing the bias field from the High-B chamber.

2.3 Modifying the Zeeman Slower

The modified Zeeman slower will use the large drop-off magnetic field from the High-B chamber as has been mentioned. This required obtaining the magnetic field profile for the chamber so that the appropriate region could be truncated as seen in Figure 2.4. While the region looks insignificant relative to the main trap field, the bias field reaches a strength of 156 G, which is near the minimum field strength (161 G)for the ideal Zeeman slower from Equation 2.14 for $\eta = 0.792$. I used a FORTRAN code which calculates the magnetic field profile for the High-B chamber that was written by Dr. Raithel.[1,35]

The modified slower must account for the difference between the required magnetic field for an ideal Zeeman slower and the bias field from the High-B chamber. I denote this as the Target Zeeman Coil Field (Target Field) and is the field the solenoid must be able to produce for this modified slower. The relationship between the ideal, bias, and target fields is shown in Figure 2.5.

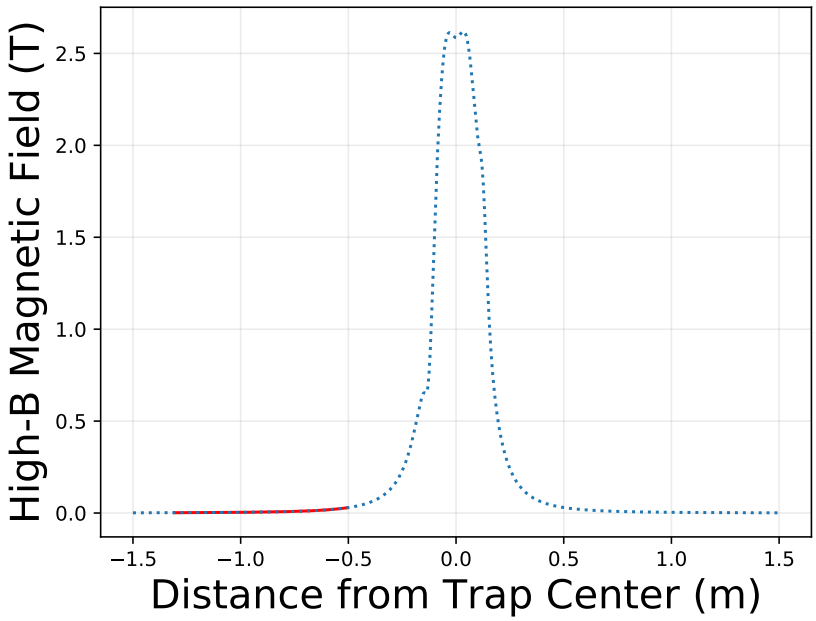

Figure 2.4: Magnetic field profile for the High-B chamber. The dotted line is the full field for up to 1.5 m away from the trap center. The solid red section corresponds to the region where the modified Zeeman slower will be placed.

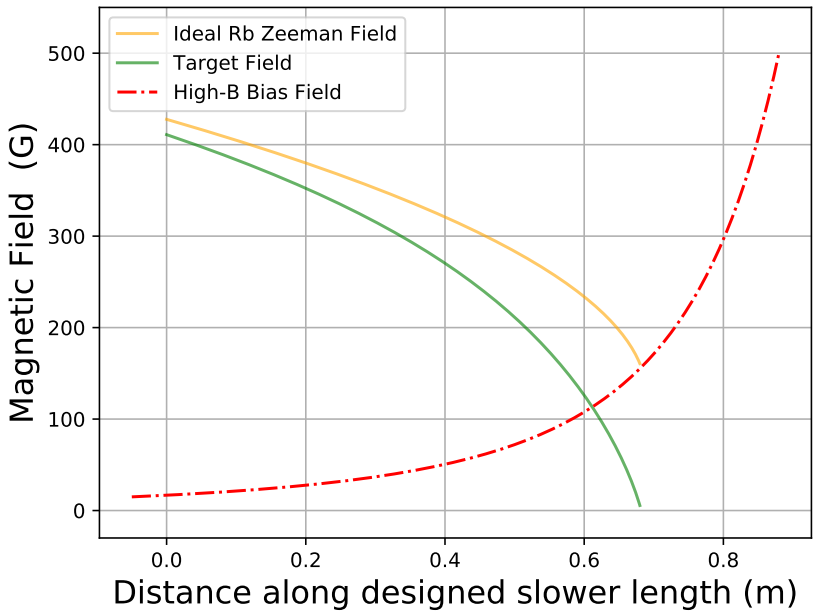

Figure 2.5: The Target Zeeman Coil Field of the modified Zeeman slower. The target field is the difference between the ideal Zeeman field and the High-B Bias field.

2.4 Generating the Desired Magnetic Field

The magnetic field for a loop of current is described by the Biot-Savart Law.[20,34]

$$\vec{\mathbf{B}}(\vec{\mathbf{r}}) = \frac{\mu_o}{4\pi} \int \frac{\vec{\mathbf{I}} \times \hat{\mathbf{r}}}{r^2} d\boldsymbol{\ell}' \tag{2.21}$$

A complete derivation of the magnetic field components for any point in space can be found in Appendix B. Since the atoms are traveling down the center of the solenoid, it is adequate to only use the axial magnetic field component and this is given by

$$B(z) = \frac{\mu_o I}{2} \frac{a^2}{(a^2 + z^2)^{3/2}} \tag{2.22}$$

where a is the radius of our loop of wire. The Target Field is generated by summing the field contributions of multiple layers of wires tightly wound into discrete solenoids. Several such solenoids are then placed in line to create the Slower. To match the Target Field as best as possible, a curve fit optimization was performed using the Python package lmfit.[36] This optimization took twelve such solenoids and varied how many wires long (the length), how many wires thick (the depth), and the current flowing through each of the solenoids in order to obtain the best possible fit for the target field. Each of these parameters was constrained in order to ensure that a valid solution was obtained.

There are additional design requirements which came up during discussions regarding the construction of the device. One of the main ones was the heat generated by the wire as current is passed through them. This was calculated using the joule heating

relation[20]

$$P = I^2 \rho \frac{l}{A} \tag{2.23}$$

where ρ is the resistivity, l is the length of wire, and A is the cross-sectional area of current flow. An alternative method of determining the joule heating that can be used for a uniform current density, J, is

$$\frac{\partial P}{\partial V} = J^2 \rho \tag{2.24}$$

which provides the power/volume for the system. For the Zeeman coils, this volume is cylindrical and excludes the volume of the inner vacuum chamber. These heating power calculations meant some additional work had to be done to find a good balance between cost, heat, and diameter of wire used for the magnet coils. It was determined that using wire of approximately 15/16 AWG in size (corresponding to roughly 1.5 mm diameter) provided the best balance between these variables. The remaining considerations were primarily issues that did not change the process of obtaining a solution and will be discussed in Chapter 3.

Chapter 3: Results

As previously mentioned in the Methods section, I need to generate a magnetic field which consists of the difference between the ideal Zeeman slower field and the bias field from the High-B chamber, as seen in Figure 2.5. Here, I discuss the modeling, optimization, design constraints/considerations, and how they contributed to the final design. I begin with the results and work through the required design aspects, and then I describe the difficulties in coding for optimization as well as many of the methods I utilized to reduce the computational load.

3.1 Optimized Zeeman Coil Results

The magnetic field is generated by running current through copper wire wrapped around a vacuum tube with a 1 inch outer diameter. The length of the solenoid is approximately given by Equation 2.16, as additional loops of wrapped wire were allowed on either side of the designed length, L, to serve as input and extraction coils. The input coil needs to bring the magnetic field up to strength for the slowing process to start but also needs to break the adiabaticity requirement so no slowing occurs outside the designed length. There will be atoms at resonance during this initial region, but they should break adiabaticity before the main slowing process begins.

The slower is designed for atoms with an initial velocity of 350 m/s to remain nearly resonant throughout the slowing process. If there is additional slowing before the atoms reach the designed starting point, it would be equivalent to having a slightly longer

designed slower with a slightly higher initial velocity. A sharp initial gradient prevents the slowing process from starting until the atoms reach the designated starting point of the slower.

The extraction coil similarly serves to break the adiabatic requirement for a long enough region that the atoms traveling with our ~ 20 m/s High-B capture velocity will be too far Zeeman detuned for the Doppler detuning to bring them close enough to resonance to allow additional unwanted slowing to take place.

Magnetic fields follow the principle of superposition, so we can add up the magnetic field contributions of single loops of wire as described by Equation 2.21. Before an attempt to fit our target field can be made, a model for the shape of the Zeeman slower must be determined. We decided to go for a more modular approach of several discrete, smaller solenoids, which give the overall slower a tapered shape. This would allow us to create several different field profiles by changing the currents passing through the solenoids. This would allow slowing of multiple species of atoms with a single device. The solenoids were modeled in Python by taking a single loop of wire, and the magnetic field it generates, and adding up consecutive loops in two ways: stacking and adjacent.

The stacking loops effectively generated a disk of current, and the magnetic field contribution for each loop accounted for the increasing radius as more wires were stacked up. These disks were then stacked adjacently for the length of that solenoid section. This secondary addition took advantage of the symmetry inherent in the axial magnetic field for a loop of current.

Each of these solenoids have their own uniform current density, based on how much current passes through it. While the current density is uniform for an individual solenoid, the shape of each solenoid is allowed to vary based on the length (in units of wire diameters) and thickness (in units of wire diameters). This allows several degrees of freedom, as we can vary the following:

1. The number of solenoids used.
2. The length of each individual solenoid.
3. The thickness of each solenoid (radius).
4. The amount of current passing through each solenoid.
5. The overall length of the slower.
6. The diameter of the copper wire.

These are the parameters which were allowed to vary to produce the final optimized solution from the Python model I generated. The final design used 20 solenoids, a wire diameter of 1.5 mm, and was optimized using the lmfit package.[36] The results are seen in Table 3.1.

Table 3.1: Solenoid Parameters for Modified ^{85}Rb Zeeman Slower Design

Sol. Index	Sol. Thickness (# wires)	Sol. Outer Rad (m)	Sol. Thickness (Exc. Vac)	Sol. Len(# wires)	Sol. Len (m)	Wire Len (m)	Rb no bias Current (A)	Rb with bias Current (A)
0	16	0.0367	0.024	10	0.015	18.7993	5.4997	5.3027
1	15	0.0352	0.0225	25	0.0375	43.1773	3.2542	3.1212
2	15	0.0352	0.0225	25	0.0375	43.1773	3.1648	3.0207
3	15	0.0352	0.0225	25	0.0375	43.1773	3.0936	2.9353
4	14	0.0337	0.021	25	0.0375	39.4741	3.1582	2.9763
5	14	0.0337	0.021	25	0.0375	39.4741	3.1062	2.9042
6	14	0.0337	0.021	25	0.0375	39.4741	3.0540	2.8283
7	13	0.0322	0.0195	25	0.0375	35.8888	3.1247	2.8612
8	13	0.0322	0.0195	25	0.0375	35.8888	3.0634	2.7673
9	13	0.0322	0.0195	25	0.0375	35.8888	2.9988	2.6635
10	12	0.0307	0.018	25	0.0375	32.4212	3.0621	2.6641
11	12	0.0307	0.018	25	0.0375	32.4212	3.0067	2.5485
12	11	0.0292	0.0165	25	0.0375	29.0715	3.0670	2.5138
13	11	0.0292	0.0165	25	0.0375	29.0715	2.9630	2.3250
14	11	0.0292	0.0165	25	0.0375	29.0715	2.8386	2.0971
15	10	0.0277	0.015	25	0.0375	25.8396	2.8860	1.9565
16	9	0.0262	0.0135	25	0.0375	22.7255	2.9198	1.7398
17	9	0.0262	0.0135	25	0.0375	22.7255	2.7126	1.2944
18	8	0.0247	0.012	25	0.0375	19.7292	2.6055	0.7330
19	7	0.0232	0.0105	39	0.0585	26.2871	2.1610	-0.4556

We see in Table 3.1 that the average current for the optimized solution, excluding the input coil, is approximately 3 A. We can see the resulting magnetic fields for these Zeeman coil solutions plotted with respect to the ideal, bias, and modified Zeeman coil fields in Figures 3.1 and 3.2. If we sum up the lengths of each solenoid (wide), we get the slower length to be 0.7485 m. The discrepancy between the design length (0.68 m), which is based on η, and this length (0.7485 m) comes from allowing the coils to extend beyond the length of the slower on both sides. This is particularly important for the input side of the slower to ensure the magnetic field is at the desired strength for the slowing process at that point. In adding the length of each loop of wire in the solution, the total amount of

copper wire is 644 m. However, this value assumes each loop is independent of each other, excluding slight overlaps between loops, so the total amount of wire length needed will be higher.

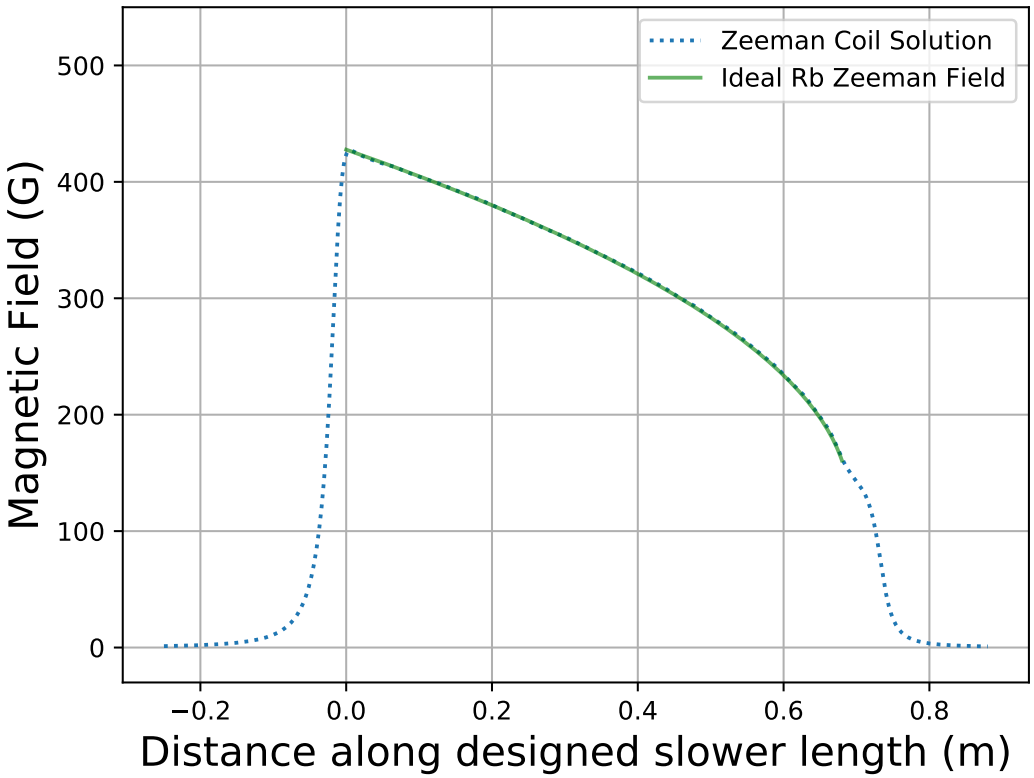

Figure 3.1: Curve fit for ideal Zeeman slower. The optimized curve fit solution for the ideal Zeeman slower is shown by the dotted line in comparison to the ideal Zeeman magnetic field for $\eta = 0.792$. Parameters are as shown in Table 3.1.

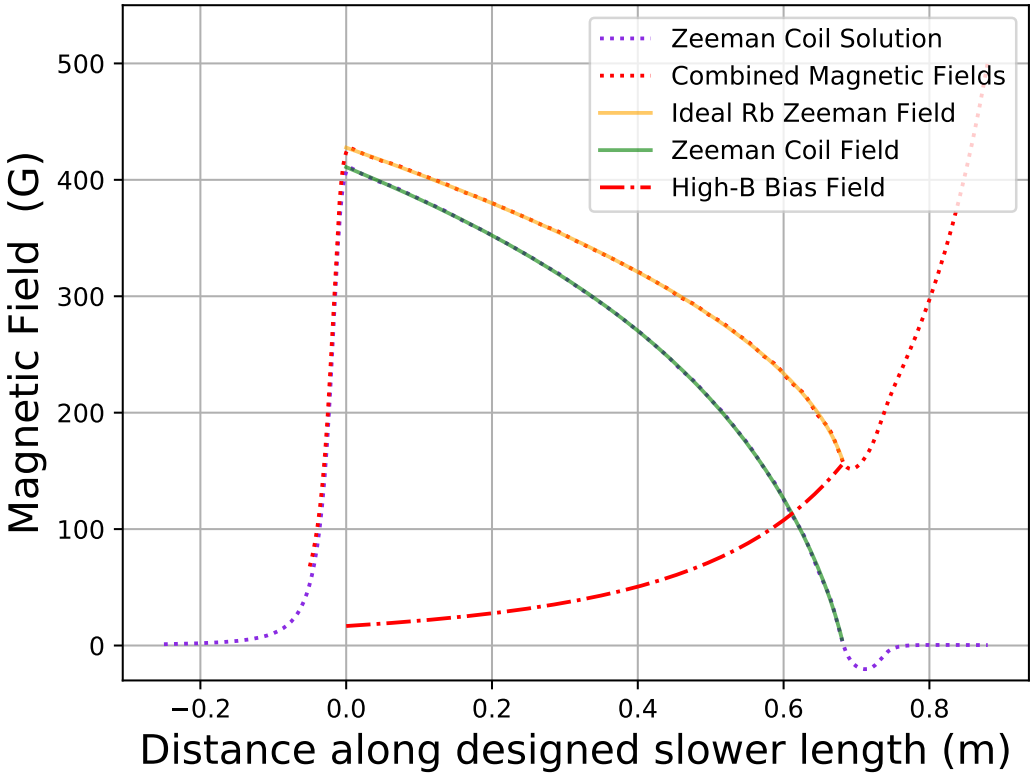

Figure 3.2: Curve fit for modified Zeeman slower. The optimized curve fit solution for the modified Zeeman slower is shown by the dotted line in comparison to the ideal Zeeman magnetic field for $\eta = 0.792$. Parameters are as shown in Table 3.1. The red dotted line shows the total contribution in magnetic field from the Zeeman Coils and the High-B field.

We can see in Figure 3.3 that both rubidium designs adhere to the adiabatic following condition limit (as defined in Equation 2.20) for the duration of the slower. The flat section of the plot corresponds to a resonant velocity of 20 m/s, which is the capture velocity for the High-B chamber. While a typical Zeeman slower is utilized for trapping at a magnetic zero point in a standard MOT setup, our slower outputs into a magnetic field with a strong gradient. We observe this by the sharp spike upwards in the gradient after the region of the slower. We use this to our advantage to help break from the slowing process.

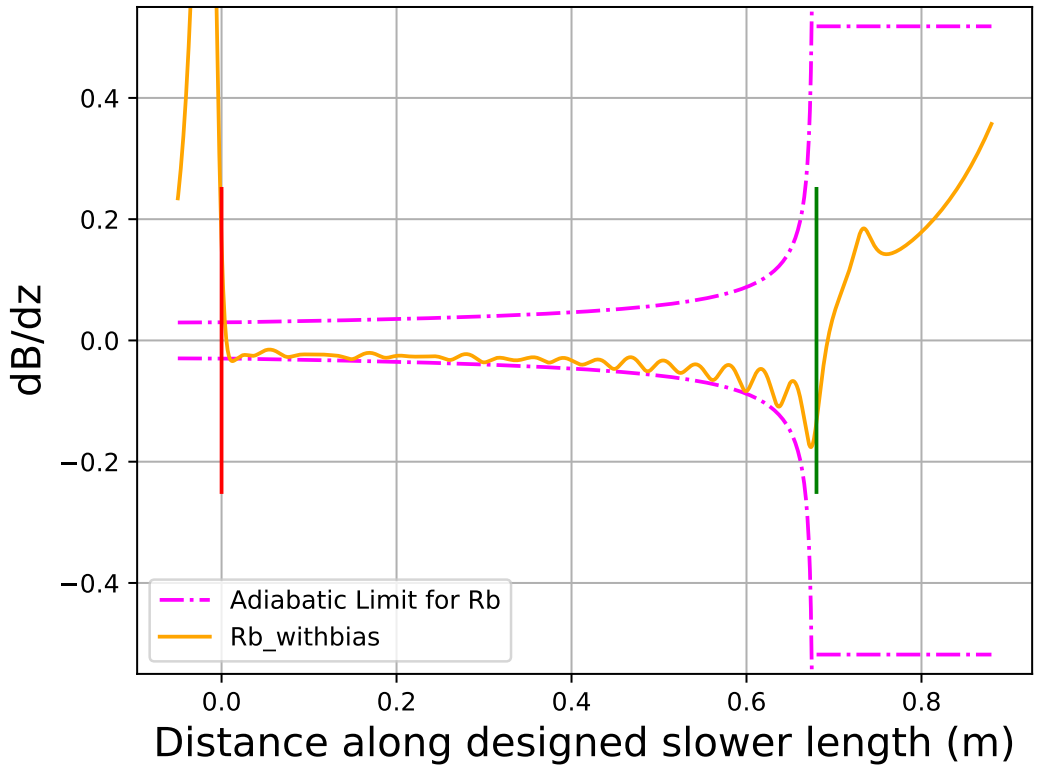

Figure 3.3: Adiabaticity of modified Zeeman slower. The gradient of the modified Zeeman coil solution fields in comparison to the maximum adiabaticity as given in Equation 2.20 (shown in purple). Any point where the gradient surpasses the adiabatic limit causes atoms in resonance at that velocity (or faster) to drop out of the slowing process as they will be too far detuned from resonance.

An additional solenoid, called the extraction coil, is placed at the end of the slower to generate a significant magnetic field gradient, forcing the atoms out of the slowing process. Figure 3.4 illustrates how the extraction coil forces the atoms out of the adiabaticity. Additional tuning of this extraction coil will be done during operation of the experiment.

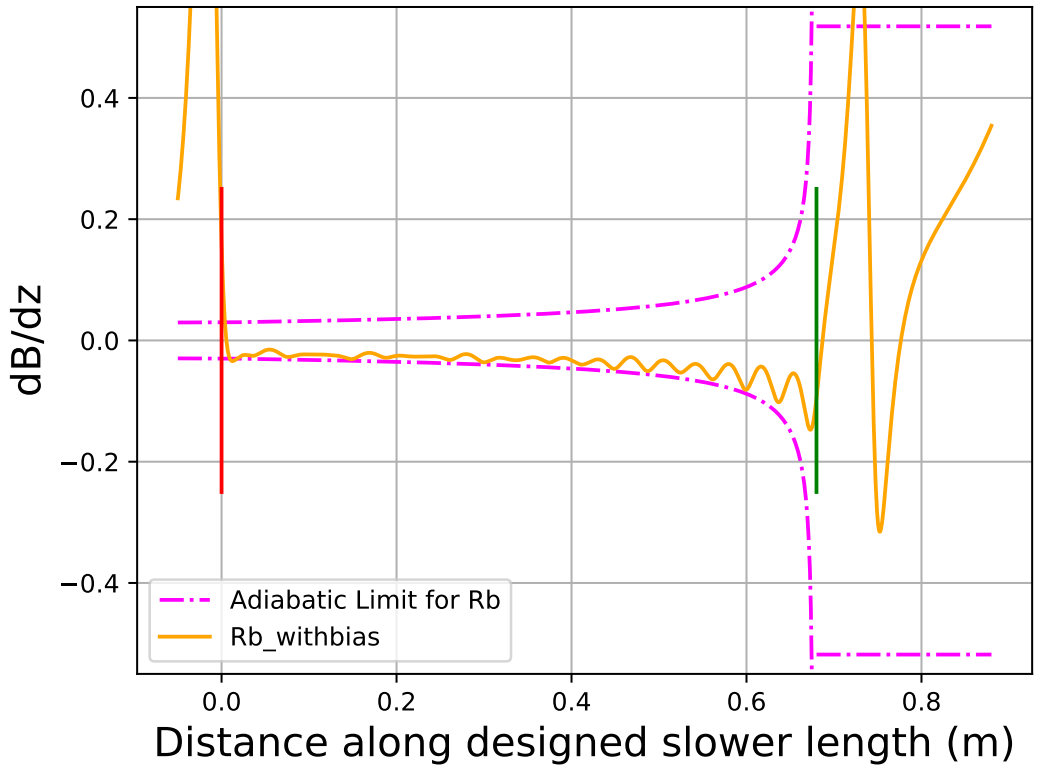

Figure 3.4: Adiabaticity of the modified Zeeman slower including extraction coil. The high gradient of the extraction coil forces the atoms to quickly break free from the slowing process. This is indicated by the spike in gradient after the green bar, which signifies the designed end of the slowing process.

Copper wire is typically sold by the pound (which typically has a conversion factor of 125 ft/lb). We went with 16 AWG (corresponding to wire diameter of 1.291 mm) Heavy GP/MR-200 MW35C/200C insulated copper wire from BAE Wire & Insulation. The total length of copper wire is proportional to the diameter and is dependent on the total cross sectional area. Several different wire diameters were tested using the algorithm, and the 16 AWG wire proved the best when it came to minimizing both the heat generation and total length of wire required. This copper wire is coated in a Polyester/Polyamide-imide shell

which will electrically isolate each coil wrap and prevent shorts between layers. The coating is rated up to 200°C, which is above the expected temperature limit of the slower. The Biot-Savart calculations use a wire diameter of 1.5 mm, but the difference in thickness from 16 AWG wire (0.209 mm) will be made up by applying a thin coating of epoxy resin between the layers of wire to help maintain the shape and positioning of the loops.

Smaller wire can be used and would reduce the current required by adding more loops per length of the slower. This will also increase the total amount of wire required and is likely to increase the heat generation due to the smaller cross-section of the wire. One of our design goals was requiring less than 6 A of current within the system.

The total joule heating was calculated using two different methods. The first method used Equation 2.23 and added up the power contribution from each individual wire from each solenoid. This gave a total joule heating power of 59 W. The second method uses 2.24 and is equivalent to approximating the cross sectional area for the current to be a rectangle based on the total length and width of each solenoid. The second method yielded a joule heating power of 25.5 W. This difference is to be expected as the same amount of current is spread out over a larger cross sectional area for the second method as it assumes the current is flowing through the area in between the wires. These two values provide rough boundaries to what we should expect from the heat generation as the actual system should fall somewhere between these ideal cases. As the inner wires are effectively sealed by the outer layers, the contribution from the inner layers is approximated to be that of a solid cylinder.

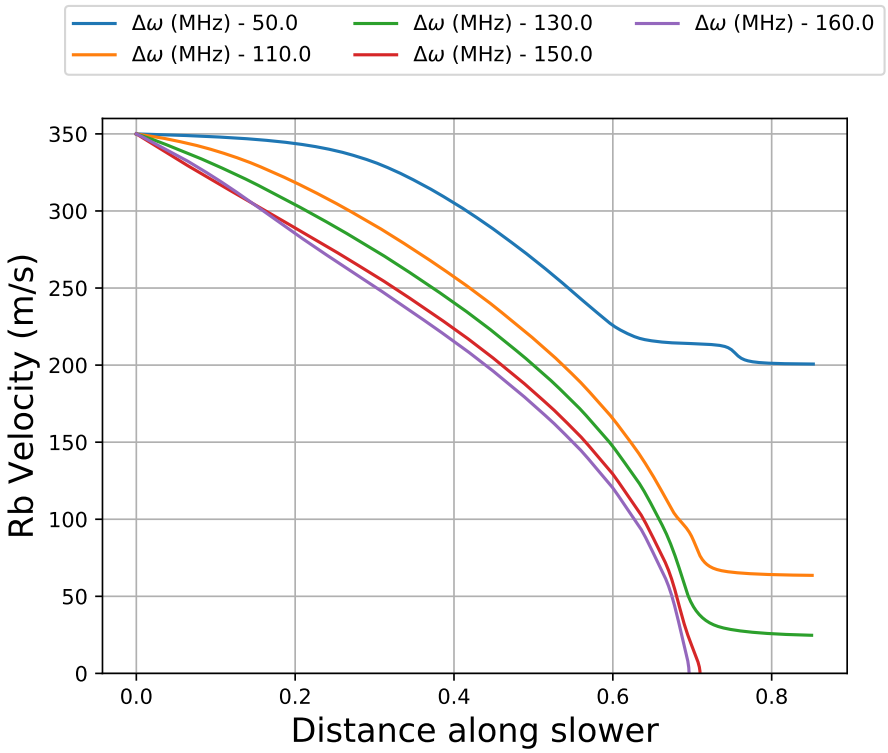

Figure 3.5: Numerical integration of velocity for multiple detuning values. This numerical integration of the force equation provides a positional velocity curve using the Fourth-Order Runge-Kutta approximation and coded in Python. A laser detuning near 130 MHz will produce atoms that have an initial velocity of 350 m/s with the proper capture velocity of ∼20 m/s. This illustrates the sensitivity of the output velocity to the detuning frequency of the slowing laser.

As a final check to ensure that the magnetic field generated by the Zeeman slower design would work as intended, a final numerical integration using the Runge-Kutta method to the fourth order was used for the acceleration from Equation 2.1, where the position and velocity are obtained by integration, but the positional magnetic field values are fed in from the Zeeman coil field. Figure 3.5 shows the velocity curves for several different detuning values, $\Delta\omega$. The field was designed for a detuning of $\Delta\omega = 150$ MHz between the laser frequency and the zero-field, zero-velocity atomic transition line and

would require the slowing process to stop precisely at the designed position of 0.68 m along the slower. Figure 3.5 shows that using such a detuning would stop all atoms with an initial velocity of 350 m/s, meaning fewer atoms will be provided for the High-B than an optimized design can provide.

The effects that incorporating the extraction coil into the model has on the adiabaticity and velocity of the atoms can be seen in Figures 3.4 and 3.6, respectively. When the gradient surpases the adiabatic limit due to the extraction coil, roughly around 0.75 cm, we see in Figure 3.6 that all atoms with this initial velocity, regardless of the detuning parameter, will cease slowing.

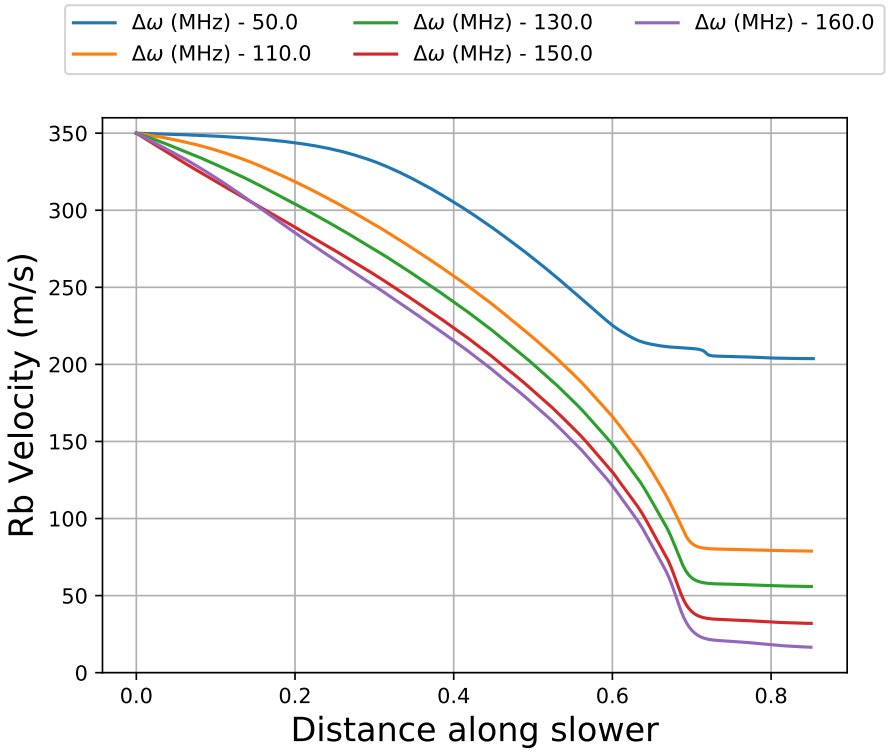

Figure 3.6: Numerical integration of velocity with extraction coil. Similar to Figure 3.5, we see the atoms all cease slowing when adiabaticity is broken by the extraction coil. This provides the fine tuning for the output velocity through the laser detuning.

Fortunately, the detuning parameter is experimentally determined so we are free to change it as required. When the extended field is taken into account, the laser detuning should be closer to 130 MHz in order to produce atoms with the goal velocity of 18.5 m/s. The extraction velocity is highly sensitive to variations of the detuning parameter. With the addition of an extraction coil, the detuning that corresponds to our capture velocity is shifted higher, closer to 160 MHz, to accommodate the increased Zeeman shift at the extraction.

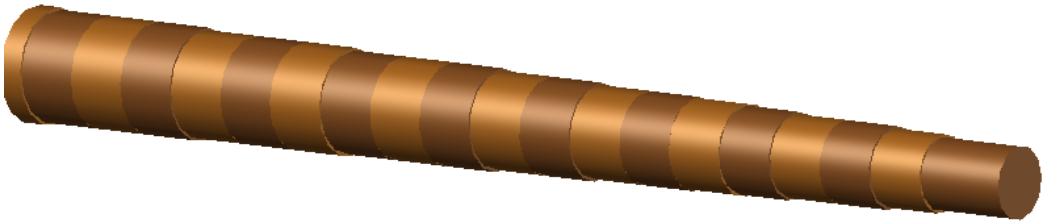

Figure 3.7: AutoCAD model of the modified Zeeman slower design. The shaded regions indicate the different solenoids.

Once the design became finalized, it was modeled in AutoCAD, as seen in Figure 3.7.

3.2 It Came From Python

As I mentioned earlier in the Results section, I had to optimize a system with many bounded, constrained, and interconnected variables. This is not an easy task to accomplish. After the first few unsuccessful attempts to create my own optimizer for these parameters, I developed a mathematical model for the general function that I needed to optimize in terms of my generated magnetic field, B_{Gen},

$$B_{Gen}(z) = \sum_{m=1}^{N} I_m * (\sum_{i=SL_{m-1}}^{SL_m} B(x_i)) \tag{3.1}$$

with I_m being the mth of N solenoids, SL_m is the wire index position, $SL_0 = 0$ for completeness, and $B(x_i)$ is the total magnetic field contribution for the x_i wires deep at that particular location. I then attempted to use some of the built-in SciPy functions such as curve fit, optimize, and minimize, but none of these are able to handle the fact that, as the length of each solenoid was changed, the next solenoid needed to move so as remove any gaps or overlaps created. I eventually came across the lmfit package which adds the freedom of bounds, constraints, and even expressions between the model to optimize. For the actual optimization algorithm that lmfit used, I chose Adaptive Memory Programming for Global Optimization (ampgo), rather than the standard least squares or Nelder-Mead methods. The ampgo method provided the highest quality solutions in the least amount of time (between 1-2 hours per solution). While the typical least squares method could often provide solutions in a few minutes (given good initial parameters), these fits are not global optimizations and often can be significantly improved. The global nature of ampgo in attempting to find the absolute best fit possible was an influencing factor in its use.

As I mentioned previously, I used the symmetry of the magnetic field and clever indexing to slice off the section of this field that would correspond to the current loop being shifted from a global origin. To prevent issues with losing far away contributions, these $B(x_i)$ fields ranged up to 2 meters away along the optical axis of the slower. To further reduce the computation, $B(x_i)$ was pulled from an array which contained the pre-calculated

magnetic field data for a single wire position with i layers deep (See Figure 3.8). This means that while there were 40,000 data points per element in this array, it would only take computational time when the program was first ran and merely be called as an object each time a solenoid changed its physical parameters during the optimization process.

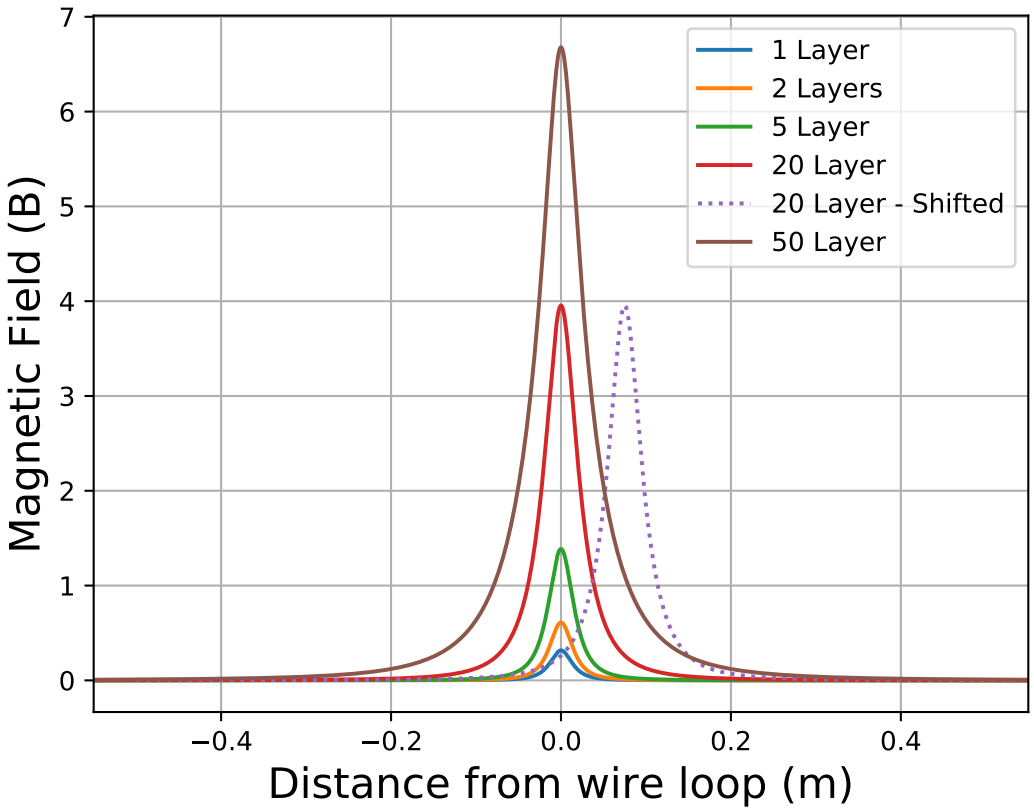

Figure 3.8: Magnetic field profiles for various wire thickness counts, $B(x_i)$. These magnetic field profiles are evaluated for a single wire location along the slower. This field data were pre-calculated as current normalized profiles and stored in a single massive array.

I mentioned above that the wire diameter was determined by running several iterations of the optimizer and comparing the heat output. It is important to note this meant the optimizer needed to be far more generalized than it initially was, in particular

the length of each individual coil pack had to be defined as a function based on the number of solenoids and the diameter of the wire. This was a required step because while I was able to limit the overall length of the slower, it was in such a manner that the last coil pack would be forced to make up the difference between the total length and the sum length of all the other coils. In other words, without this additional limitation to the length of each solenoid, there was nothing preventing the optimizer from surpassing the designated total length before it reached the final solenoid.

The quality of a curve fit or optimization tends to heavily rely upon the initial fit parameters. While I initially had my algorithm import an external csv parameter file, I eventually found a more generalized method that provided a fairly decent initial fit, regardless of wire diameter or number of solenoids. Exploiting the shape of the expected magnetic field (square root plus an offset as per Equation 2.10), I divided my total slower into equal length solenoids but applied the same such form of $A_n = B + C * \sqrt{1 - n/N}$. This equation allows for both the current and depth parameters to have a form similar to that of the desired magnetic field that they generate. Using this equation, I was then able to generate initial parameters for the current and solenoid depths which would be congruent to the overall field shape. It is very likely that optimizing such a general solution could generate a great quality Zeeman field, but that is outside the scope of this project.

The algorithm and methods I have defined do not just solve the rubidium Zeeman slower design problem, they are able to create any desired magnetic field given any bias field shape/strength. The only limiting factors involve ensuring the fields line up properly

and use the same positional step sizes.

I created a Python model which optimized the curve fit for the magnetic field profile of a Zeeman slower using the lmfit package. The model, which I coded from scratch, used the Biot-Savart law to calculate the magnetic field for a loop of current carrying wire along the axis of symmetry. The ideal Zeeman field was composed of two separate parts: the fall-off bias field from the High-B and the field generated by a set of independent solenoids. Using 20 solenoids, I was able to generate a field that never differed by more than 4G from the ideal field. I verified the slower would work by numerically integrating the force acting on the atoms as well as checked that the field never exceeded the adiabatic limits described in Chapter 2.

While I have shown that the slower will function exactly on the symmetry axis of the solenoids, the off-axis effects would be interesting to model and compare. My computational model is capable of this calculation, but the simplicity of the axial form of the Biot-Savart law improved computational time during the optimization process.

As a final code related note, all of the code mentioned here, except for the packages used, was written by me for this project but may be found at https://github.com/Jehiren/ZeemanCode.

Chapter 4: Conclusion

4.1 Designing a Modified Zeeman Slower

There are many interesting phenomena that occur when plasmas are contained in strong magnetic fields, especially in fields stronger than 1 T, as can be obtained in the High-B trap. In order to study these plasmas, a sufficiently high flux of slowed atoms must be provided into the trapping apparatus. The experiments previously conducted in the High-B chamber were done with a lower plasma density as the atom source used, the LVIS, could only produce an atomic flux of roughly 10^7 atoms/s. This low plasma density limited the observation of low probability events, such as Three-Body Recombination. In order to provide significantly greater atomic flux, this LVIS is to be replaced by a modified Zeeman slower. Zeeman slowers are well studied devices which have been proven to be capable of providing atomic flux upwards of 10^{12} atoms/s.

I have designed a modified Zeeman slower that will provide a constant flux of slowed atoms into the High-B chamber. This modified slower incorporates the significant fringe field of the High-B chamber into its magnetic field profile. Zeeman slowers typically are used for standard MOTs, which typically trap in a region with zero magnetic field. The modified slower must be able to incorporate the non-homogeneous High-B bias field and produce a steady flux of slowed and cooled atoms which can be trapped within the High-B trap.

As the magnetic field continues to sharply increase in the region after the slower,

there are additional considerations that are required regarding which cycling transition can be utilized. While an increasing field slower would be ideal, as it would match the natural field profile of the High-B trap field (increases toward the trap center), the $|F = 3, m_F = -3\rangle$ and $|F' = 4, m_{F'} = -4\rangle$ are high-field seeking states which will accelerate towards stronger magnetic fields. Atoms in these states are not trappable due to this acceleration.

My modified design is optimized to work both with and without the High-B fringe field using a modular design consisting of multiple adjacent solenoids. Each of these solenoids, 20 in total, had three free parameters to optimize: length, depth, and current. My Python algorithm then performed an optimization to obtain the best possible fit for the system. The total field must meet the adiabatic requirement condition, which limits the gradient of the field based on the position and velocity for each point along the slower.

I used my Python algorithm to obtain solutions for strontium atoms, but those are poor in quality as they used a design parameter of $\eta = 0.077$, meaning a significant portion of the atoms would be lost due to the expansion of the atomic beam over the longitudinal distance of the slower. An ideal strontium slower has a length of approximately 7 cm as the maximum deceleration of strontium is roughly 10 times greater. Attempting to modify the rubidium slower to work with strontium is a poor fit. Additionally, this optimizer can recreate any magnetic field profile, within reason, using these solenoids.

With the completed design parameters, I then modeled the slower in AutoCAD. All that remains is figuring out the fine details of constructing the slower in terms of parts,

labor, and possible design alterations that allow for ease of use of the slower in the lab.

4.2 Future Work

Now that a theoretical design has been completed and proven to meet the technical requirements, the next steps are to physically build and test the slower. With all construction situations, there are typically unforeseen changes that must be made to accommodate a functional lab environment. There were several minor considerations that were incorporated into the slower design throughout the project, but there is a major revision required with the algorithm that will fundamentally change how the solution is generated.

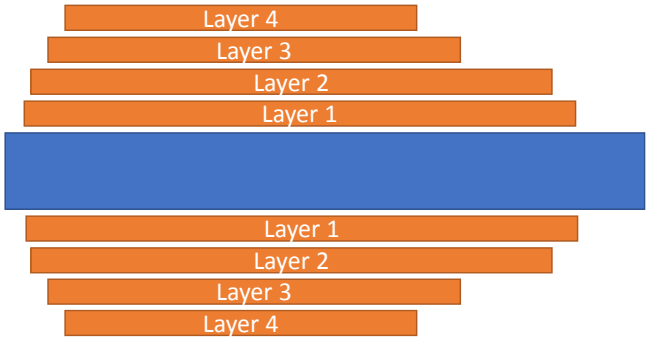

Figure 4.1: Model for layered design approach. This new design approach will attempt to generate a solution using stacked layers rather than several discrete smaller solenoids.

The design change is to consider stacking consecutive layers of wire along the entire slower body as illustrated in Figure 4.1. The solution presented above in Chapter 3 utilized 20 independent power supplies to provide the DC current to pass into the wires. This was not a feasible design as it meant there were now 20 independent variables that could all be

adjusted, which is simply too much to allow for fine tuning. In comparison to the difficulties of wiring the 20 solenoid currents, this layered design would be far simpler.

By removing strontium from the design considerations, the ideal situation can be reduced to a single current passing through the main body of the slower solenoid. This would provide a tunable field where adiabaticity should be maintained even with minor adjustments to the overall current. This would change which atoms are traveling at resonant velocities during the slowing process, allowing fine tuning for the output velocity of the slower. The addition of an extraction coil is still a requirement to ensure adiabaticity is broken in a controlled manner, halting the slowing process once atoms reach the desired speed. These changes are currently in progress and a finalized design should completed before August 2019.

Bibliography

[1]J. R. Guest, J.-H. Choi, E. Hansis, A. P. Povilus, and G. Raithel, "Laser Cooling and Magnetic Trapping at Several Tesla", Phys. Rev. Lett. **94**, 073003 (2005).

[2]J. Guest and G. Raithel, "High-|m| Rydberg states in strong magnetic fields", Phys. Rev. A **68**, 052502 (2003).

[3]J.-H. Choi, J. R. Guest, A. P. Povilus, E. Hansis, and G. Raithel, "Magnetic trapping of long-lived cold Rydberg atoms", Phys. Rev. Lett. **95**, 243001 (2005).

[4]J.-H. Choi, B. Knuffman, X. Zhang, A. Povilus, and G. Raithel, "Trapping and evolution dynamics of ultracold two-component plasmas", Phys. Rev. Lett. **100**, 175002 (2008).

[5]E. Paradis, S. Zigo, K. Hu, and G. Raithel, "Characterization of laser cooling in a high-magnetic-field atom trap", Phys. Rev. A **86**, 023416 (2012).

[6]E. Paradis, S. Zigo, and G. Raithel, "Highly polar states of rydberg atoms in strong magnetic and weak electric fields", Phys. Rev. A **87**, 012505 (2013).

[7]E. Paradis, "High-Magnetic-Field Rydberg Atom Interactions", PhD thesis (University of Michigan, 2013).

[8]F. Robicheaux, "Three-body recombination for electrons in a strong magnetic field: magnetic moment", Phys. Rev. A **73**, 033401 (2006).

[9]M. E. Glinsky and T. M. O'Neil, "Guiding center atoms: Three-body recombination in a strongly magnetized plasma", Phys. Fluids B **3**, 1279–1293 (1991).

[10]Z. Lu, K. Corwin, M. Renn, M. Anderson, E. A. Cornell, and C. Wieman, "Low-velocity intense source of atoms from a magneto-optical trap", Phys. Rev. Lett. **77**, 3331 (1996).

[11]G. Bannasch, T. Killian, and T. Pohl, "Strongly coupled plasmas via rydberg blockade of cold atoms", Phys. Rev. Lett. **110**, 253003 (2013).

[12]K. Singer, J. Stanojevic, M. Weidemüller, and R. Côté, "Long-range interactions between alkali Rydberg atom pairs correlated to the ns–ns, np–np and nd–nd asymptotes", J. Phys. B **38**, S295 (2005).

[13]S. Ichimaru, "Strongly coupled plasmas: high-density classical plasmas and degenerate electron liquids", Rev. Mod. Phys. **54**, 1017 (1982).

[14]C. Slowe, L. Vernac, and L. V. Hau, "High flux source of cold rubidium atoms", Rev. Sci. Instrum. **76**, 103101 (2005).

[15]T. Yang, K. Pandey, M. S. Pramod, F. Leroux, C. C. Kwong, E. Hajiyev, Z. Y. Chia, B. Fang, and D. Wilkowski, "A high flux source of cold strontium atoms", EU Phys J. D **69**, 226 (2015).

[16]H. Metcalf and P. van der Straten, *Laser Cooling and Trapping*, Graduate Texts in Contemporary Physics (Springer New York, 2012).

[17]W. D. Phillips and H. Metcalf, "Laser deceleration of an atomic beam", Phys. Rev. Lett. **48**, 596–599 (1982).

[18]R. Swenumson and U. Even, "Continuous flow reflux oven as the source of an effusive molecular Cs beam", Rev. Sci. Instrum. **52**, 559–561 (1981).

[19]B. E. Saleh and M. C. Teich, *Fundamentals of Photonics* (Wiley, 2007).

[20]D. Griffiths, *Introduction to Electrodynamics*, Pearson International Edition (Pearson Prentice Hall, Upper Saddle River, NJ, 2013).

[21]D. Griffiths, *Introduction to Quantum Mechanics*, Pearson international edition (Pearson Prentice Hall, Upper Saddle River, NJ, 2005).

[22]J. S. Townsend, *A Modern Approach to Quantum Mechanics* (University Science Books, 2000).

[23]B. Ohayon and G. Ron, "New approaches in designing a Zeeman Slower", J. Instrum. **8**, P02016 (2013).

[24]B. Ohayon and G. Ron, "Investigation of different magnetic field configurations using an electrical, modular Zeeman slower", Rev. Sci. Instrum. **86**, 103110 (2015).

[25]C. J. Dedman, J. Nes, T. Hanna, R. Dall, K. Baldwin, and A. Truscott, "Optimum design and construction of a zeeman slower for use with a magneto-optic trap", Rev. Sci. Instrum. **75**, 5136–5142 (2004).

[26]R. R. Mhaskar, "Toward an atom laser: Cold atoms in a long, high-gradient magnetic guide", PhD thesis (University of Michigan, 2008).

[27]G. Reinaudi, C. B. Osborn, K. Bega, and T. Zelevinsky, "Dynamically configurable and optimizable zeeman slower using permanent magnets and servomotors", J. Opt. Soc. Am. B **29**, 729–733 (2012).

[28]R. Napolitano, S. Zilio, and V. Bagnato, "Adiabatic following conditions for the deceleration of atoms with the Zeeman tuning technique", Opt. Commun. **80**, 110–114 (1990).

[29]S. Mayer, N. Minarik, M. Shroyer, and D. Mclntyre, "Zeeman-tuned slowing of rubidium using σ^+ and σ^- polarized light", Opt. Commun. **210**, 259–270 (2002).

[30]V. Bagnato, A. Aspect, and S. Zilio, "Study of laser deceleration of an atomic beam by monitoring the fluorescence along the deceleration path", Opt. Commun. **72**, 76–81 (1989).

[31]T. E. Barrett, S. W. Dapore-Schwartz, M. D. Ray, and G. P. Lafyatis, "Slowing atoms with σ- polarized light", Phys. Rev. Lett. **67**, 3483 (1991).

[32]W. H. Wing, "On neutral particle trapping in quasistatic electromagnetic fields", Progress in Quantum Electronics **8**, 181–199 (1984).

[33]I. R. Hill, Y. B. Ovchinnikov, E. M. Bridge, E. A. Curtis, S. Donnellan, and P. Gill, "A simple, configurable, permanent magnet Zeeman Slower for Sr", in European frequency and time forum (eftf), 2012 (IEEE, 2012), pp. 545–549.

[34]A. Zangwill, *Modern electrodynamics* (Cambridge University Press, 2013).

[35]G. Raithel, *Magnetic Field Calculations for CYROMOT High-B chamber*, Personal correspondence to provide previously created FORTRAN code. 2018.

[36]M. Newville, T. Stensitzki, D. B. Allen, and A. Ingargiola, *LMFIT: Non-Linear Least-Square Minimization and Curve-Fitting for Python*, Sept. 2014.

APPENDICES

Appendix A: Hyperfine Structure

To calculate the hyperfine structure of rubidium, we take our total Hamiltonian to be the sum of the hyperfine and field interaction Hamiltonians, $\hat{\mathbf{H}}_{tot} = \hat{\mathbf{H}}_{hfs} + \hat{\mathbf{H}}_{int}$, where $\hat{\mathbf{H}}_{int}$ is the Hamiltonian for the interaction with an external field and is given along the axis of quantization (taken to be the direction of the magnetic field, typically the z component),

$$\hat{\mathbf{H}}_{int} = \frac{\mu_B}{\hbar}(g_s\hat{\mathbf{S}}_z + g_L\hat{\mathbf{L}}_z + g_I\hat{\mathbf{I}}_z)B_z \tag{A.1}$$

where μ_B is the Bohr Magneton, g_s, g_L, and g_I, are the Lande g-factors for the Spin, Orbital, and Nuclear angular momenta, respectively. $\hat{\mathbf{S}}_z, \hat{\mathbf{L}}_z$, and $\hat{\mathbf{I}}_z$ are the z-component operators for the Spin, Total, and Nuclear angular momenta, respectively. The total angular momentum is defined as the vector sum of these three components and denoted by $\hat{\mathbf{F}} = \hat{\mathbf{S}} + \hat{\mathbf{L}} + \hat{\mathbf{I}}$. In the absence of a magnetic field, the spin and orbital angular momenta have no interactions and can be combined into $\hat{\mathbf{J}}$, which is the total angular momentum of the electron (excluding contributions from the nucleus).

After applying the raising/lowering operators, we obtain the Clebsch-Gordon coefficients that write our $|F, m_F\rangle$ states in the $|I, m_I\rangle\,|J, m_J\rangle$ states and since we are only interested in the J=3/2 states, we will abbreviate the notation where integer kets denote $|F, m_F\rangle$ states and the non-integer kets are given (for ^{85}Rb) as $|m_I, m_J\rangle$ where I = 5/2 and J = 3/2, unless otherwise stated. Going through this process for the $5P_{3/2}$ excited state of ^{85}Rb gives us:

$F = 4$

$$|4,4\rangle = |5/2,3/2\rangle$$

$$|4,3\rangle = \sqrt{5/8}\,|3/2,3/2\rangle + \sqrt{3/8}\,|5/2,1/2\rangle$$

$$|4,2\rangle = \sqrt{5/14}\,|1/2,3/2\rangle + \sqrt{15/28}\,|3/2,1/2\rangle + \sqrt{3/28}\,|5/2,-1/2\rangle$$

$$|4,1\rangle = \sqrt{5/28}\,|-1/2,3/2\rangle + \sqrt{15/28}\,|1/2,1/2\rangle + \sqrt{15/56}\,|3/2,-1/2\rangle + \sqrt{1/56}\,|5/2,-3/2\rangle$$

$$|4,0\rangle = \sqrt{1/14}\,|-3/2,3/2\rangle + \sqrt{3/7}\,|-1/2,1/2\rangle + \sqrt{3/7}\,|1/2,-1/2\rangle + \sqrt{1/14}\,|3/2,-3/2\rangle$$

$$|4,-1\rangle = \sqrt{1/56}\,|-5/2,3/2\rangle + \sqrt{15/56}\,|-3/2,1/2\rangle + \sqrt{15/28}\,|-1/2,-1/2\rangle + \sqrt{5/28}\,|1/2,-3/2\rangle$$

$$|4,-2\rangle = \sqrt{3/28}\,|-5/2,1/2\rangle + \sqrt{15/28}\,|-3/2,-1/2\rangle + \sqrt{5/14}\,|-1/2,-3/2\rangle$$

$$|4,-3\rangle = \sqrt{3/8}\,|-5/2,-1/2\rangle + \sqrt{5/8}\,|-3/2,-3/2\rangle$$

$$|4,-4\rangle = |-5/2,-3/2\rangle$$

$F = 3$

$$|3,3\rangle = \sqrt{5/8}\,|5/2,1/2\rangle - \sqrt{3/8}\,|3/2,3/2\rangle$$

$$|3,2\rangle = -\sqrt{1/2}\,|1/2,3/2\rangle + \sqrt{1/12}\,|3/2,1/2\rangle + \sqrt{5/12}\,|5/2,-1/2\rangle$$

$$|3,1\rangle = -\sqrt{9/20}\,|-1/2,3/2\rangle - \sqrt{1/60}\,|1/2,1/2\rangle + \sqrt{49/120}\,|3/2,-1/2\rangle + \sqrt{1/8}\,|5/2,-3/2\rangle$$

$$|3,0\rangle = -\sqrt{3/10}\,|-3/2,3/2\rangle - \sqrt{1/5}\,|-1/2,1/2\rangle + \sqrt{1/5}\,|1/2,-1/2\rangle + \sqrt{3/10}\,|3/2,-3/2\rangle$$

$$|3,-1\rangle = -\sqrt{1/8}\,|-5/2,3/2\rangle - \sqrt{49/120}\,|-3/2,1/2\rangle + \sqrt{1/160}\,|-1/2,-1/2\rangle + \sqrt{9/20}\,|1/2,-3/2\rangle$$

$$|3,-2\rangle = -\sqrt{5/12}\,|-5/2,1/2\rangle - \sqrt{1/12}\,|-3/2,-1/2\rangle + \sqrt{1/12}\,|-1/2,-3/2\rangle$$

$$|3,-3\rangle = -\sqrt{5/8}\,|-5/2,-1/2\rangle + \sqrt{3/8}\,|-3/2,-3/2\rangle$$

$F = 2$

$$|2,2\rangle = \sqrt{1/7}\,|1/2,3/2\rangle - \sqrt{8/21}\,|3/2,1/2\rangle + \sqrt{10/21}\,|5/2,-1/2\rangle$$

$$|2,1\rangle = \sqrt{9/28}\,|-1/2,3/2\rangle - \sqrt{25/84}\,|1/2,1/2\rangle + \sqrt{1/42}\,|3/2,-1/2\rangle + \sqrt{5/14}\,|5/2,-3/2\rangle$$

$$|2,0\rangle = \sqrt{3/7}\,|-3/2,3/2\rangle - \sqrt{1/14}\,|-1/2,1/2\rangle - \sqrt{1/14}\,|1/2,-1/2\rangle + \sqrt{3/7}\,|3/2,-3/2\rangle$$

$$|2,-1\rangle = \sqrt{5/14}\,|-5/2,3/2\rangle + \sqrt{1/42}\,|-3/2,1/2\rangle - \sqrt{25/84}\,|-1/2,-1/2\rangle + \sqrt{9/28}\,|1/2,-3/2\rangle$$

$$|2,-2\rangle = \sqrt{10/21}\,|-5/2,1/2\rangle - \sqrt{8/21}\,|-3/2,-1/2\rangle + \sqrt{1/7}\,|-1/2,-3/2\rangle$$

$F = 1$

$$|1,1\rangle = -\sqrt{1/20}\,|-1/2,3/2\rangle + \sqrt{3/20}\,|1/2,1/2\rangle - \sqrt{3/10}\,|3/2,-1/2\rangle + \sqrt{1/2}\,|5/2,-3/2\rangle$$

$$|1,0\rangle = -\sqrt{1/5}\,|-3/2,3/2\rangle + \sqrt{3/10}\,|-1/2,1/2\rangle - \sqrt{3/10}\,|1/2,-1/2\rangle + \sqrt{1/5}\,|3/2,-3/2\rangle$$

$$|1,-1\rangle = -\sqrt{1/2}\,|-5/2,3/2\rangle + \sqrt{3/10}\,|-3/2,1/2\rangle - \sqrt{3/20}\,|-1/2,-1/2\rangle + \sqrt{1/20}\,|1/2,-3/2\rangle$$

which allows us to write our degenerate F states in the low field in terms of the $|m_I, m_J\rangle$ basis. Doing this removes needing perturbation theory as we will instead re-diagonalize the Hamiltonian at every magnetic field evaluation using python. This is the intermediate magnetic field Zeeman effect.

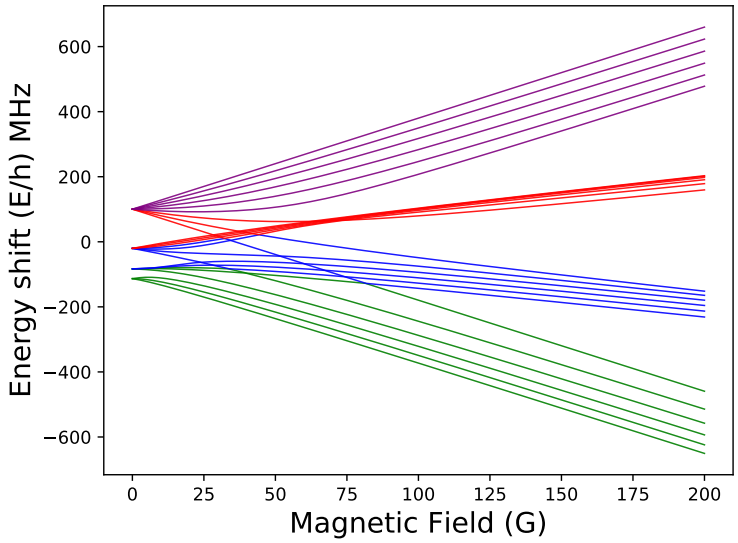

Figure A.1: Hyperfine structure for the $5P_{3/2}$ excited state of rubidium. There are 24 possible states, corresponding to the 4 $|m_J\rangle$ states {3/2, 1/2, -1/2, -3/2}, and the 6 $|m_I\rangle$ states of {5/2, 3/2, 1/2, -1/2, -3/2, -5/2}.

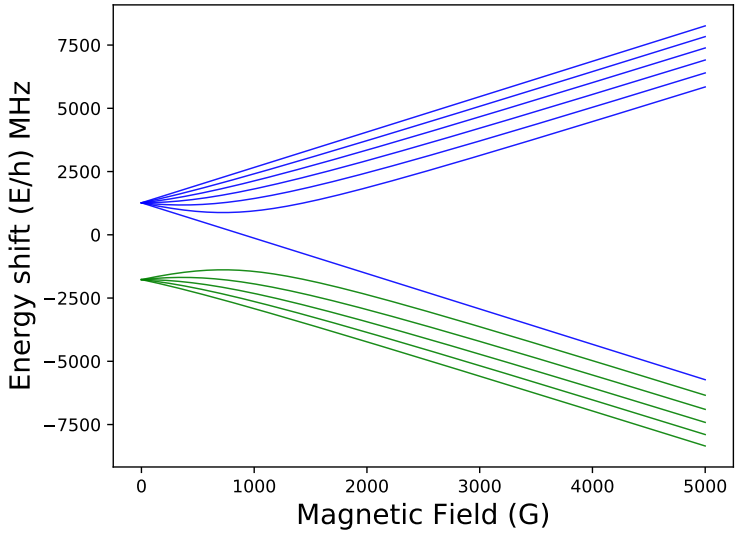

Figure A.2: Hyperfine structure for ground state of rubidium. The states start grouped by $|F, m_F\rangle$ states on the left and groups of $|m_J\rangle$ on the right. There are 12 states in total, with the seven initially on top corresponding to the $|F = 3\rangle$ state and the bottom 5 corresponding to the $|F = 2\rangle$ state.

For the $5S_{1/2}$ ground state of ^{85}Rb we have Clebsch-Gordon coefficients of:

$$F = 3$$

$$|3,3\rangle = |5/2,1/2\rangle$$

$$|3,2\rangle = \sqrt{5/6}\,|3/2,1/2\rangle + \sqrt{1/6}\,|5/2,-1/2\rangle$$

$$|3,1\rangle = \sqrt{2/3}\,|1/2,1/2\rangle + \sqrt{1/3}\,|3/2,-1/2\rangle$$

$$|3,0\rangle = \sqrt{1/2}\,|-1/2,1/2\rangle + \sqrt{1/2}\,|1/2,-1/2\rangle$$

$$|3,-1\rangle = \sqrt{1/3}\,|-3/2,1/2\rangle + \sqrt{2/3}\,|-1/2,-1/2\rangle$$

$$|3,-2\rangle = \sqrt{1/6}\,|-5/2,1/2\rangle + \sqrt{5/6}\,|-3/2,-1/2\rangle$$

$$|3,-3\rangle = \sqrt{5/8}\,|3/2,-1/2\rangle$$

$$F = 2$$

$$|2,2\rangle = \sqrt{1/6}\,|3/2,1/2\rangle - \sqrt{5/6}\,|5/2,-1/2\rangle$$

$$|2,1\rangle = \sqrt{1/3}\,|1/2,1/2\rangle - \sqrt{2/3}\,|3/2,-1/2\rangle$$

$$|2,0\rangle = \sqrt{1/2}\,|-1/2,1/2\rangle - \sqrt{1/2}\,|1/2,-1/2\rangle$$

$$|2,-1\rangle = \sqrt{2/3}\,|-3/2,1/2\rangle - \sqrt{1/3}\,|-1/2,-1/2\rangle$$

$$|2,-2\rangle = \sqrt{5/6}\,|-5/2,1/2\rangle - \sqrt{1/6}\,|-3/2,-1/2\rangle$$

We see the hyperfine structure for the ground state of rubidium in figure A.2 and the hyperfine structure for the $5P_{3/2}$ excited state in figure A.1. The states are defined by

their $|F\rangle$ quantum number in the low field (Zeeman) regime, but this breaks down due to spin-orbital decoupling at higher magnetic fields. In this higher magnetic field regime (Paschen-Back), the states are defined by the $|m_I, m_J\rangle$ where the $|m_I\rangle$ states are clustered together based on their $|m_J\rangle$ state.

Appendix B: Biot-Savart Derivation

To numerically evaluate the magnetic field from a loop of current, we break the integral of the Biot-Savart law (as seen in equation 2.21):

$$\vec{\mathbf{B}}(\vec{\mathbf{r}}) = \frac{\mu_o}{4\pi} \int \frac{\vec{\mathbf{I}} \times \hat{\mathbf{r}}}{r^2} \boldsymbol{d\ell'} \tag{B.1}$$

into the discrete contribution, dB, for a particular section of the loop, $\boldsymbol{d\ell'}$. This gives us the differential form of the Biot-Savart Law:

$$\mathbf{d}\vec{\mathbf{B}} = \frac{\mu_o \vec{\mathbf{I}} d\ell' \times \vec{\mathbf{r}}}{4\pi r^3} \tag{B.2}$$

for some wire of current, I, along a path $\boldsymbol{d\ell'}$. We use the convention that primed coordinates denote the geometry of the source points. The loop of current will be parallel to the xy-plane and offset by an amount of $\vec{\mathbf{r}}_o = (x_o, y_o, z_o)$ in standard Cartesian coordinates. We want to evaluate the magnetic field at some point P defined by the position vector $\vec{\mathbf{r}} = (x, y, z)$, which gives us a displacement vector

$$\vec{\mathbf{d}} = \vec{\mathbf{r}} - \vec{\mathbf{r}'} \tag{B.3}$$

where the source points are obtained by using a conversion from cylindrical symmetry for a circle with radius a:

$$x' = x_o + a\cos(\phi')$$

$$y' = y_o + a\sin(\phi')$$

$$z' = z_o \tag{B.4}$$

This allows us to find our displacement vector:

$$\vec{\mathbf{d}} = (x - x_o - a\cos(\phi'), y - y_o - a\sin(\phi'), z - z_o) \tag{B.5}$$

which we will substitute for r into equation B.2 above. The line integral over the loop is done by integrating over the differential vector line elements given by $\boldsymbol{d\ell'} = dx'\hat{\mathbf{x}} + dy'\hat{\mathbf{y}} + dz'\hat{\mathbf{z}}$. B_x, B_y, and B_z are the x-, y- , and z- components of the magnetic field. We can evaluate the cross product and get:

$$dB_x = \frac{\hat{\mathbf{x}}[a(z - z_o)\cos(\phi')]d\phi'}{|d|^3}$$

$$dB_y = \frac{\hat{\mathbf{y}}[a(z - z_o)\sin(\phi')]d\phi'}{|d|^3}$$

$$dB_z = \frac{\hat{\mathbf{z}}[a^2 + a(y_o - y)\sin(\phi') + a(x_o - x)\cos(\phi')]d\phi'}{|d|^3} \tag{B.6}$$

with $\left|\vec{\mathbf{d}}\right|$ being the magnitude of our displacement vector and given as:

$$\left|\vec{\mathbf{d}}\right|^2 = (x - x_o)^2 + (y - y_o)^2 + (z - z_o)^2 + a^2 + 2a[(x_o - x)\cos(\phi') + (y_o - y)\sin(\phi')] \tag{B.7}$$

where we numerically integrate around ϕ' with my Python code to determine the magnetic field for a discrete section of the magnetic field. The calculations for the loops used in the optimizer separated the loop into 20 sections. The code evaluated the magnetic field for all of the points in a Cartesian volume d^3r. This meant there would be points P being evaluated which would approach the current-carrying wire location, which blows up to infinity as $\vec{\mathbf{d}}$ approached 0. To avoid this issue during evaluation, a conditional check was made that would replace any distance smaller than a given minimum distance with that minimum distance value. This meant that any displacement less than $0.1\mu m$ was evaluated as $0.1\mu m$.

Computationally solving the Biot-Savart law in this manner allows us to avoid the issue of solving the elliptical integral obtained from attempting to determine an exact analytical solution to Equation 2.21.